NASA TECHNICAL MEMORANDUM

NASA TM X-2037

NASA TM X-2037

PERFORMANCE OF A FIXED GEOMETRY WIND TUNNEL MODEL OF AN AUXILIARY INLET EJECTOR WITH A CLAMSHELL FLOW DIVERTER FROM MACH 0 TO 1.2

by Fred W. Steffen and Albert L. Johns

Lewis Research Center
Cleveland, Ohio 44135

NATIONAL AERONAUTICS AND SPACE ADMINISTRATION • WASHINGTON, D. C. • JULY 1970

1. Report No. NASA TM X-2037	2. Government Accession No.	3. Recipient's Catalog No.
4. Title and Subtitle PERFORMANCE OF A FIXED GEOMETRY WIND TUNNEL MODEL OF AN AUXILIARY INLET EJECTOR WITH A CLAMSHELL FLOW DIVERTER FROM MACH 0 TO 1.2		5. Report Date July 1970 6. Performing Organization Code
7. Author(s) Fred W. Steffen and Albert L. Johns		8. Performing Organization Report No. E-5554
9. Performing Organization Name and Address Lewis Research Center, National Aeronautics and Space Administration, Cleveland, Ohio 44135		10. Work Unit No. 126-15 11. Contract or Grant No. 13. Type of Report and Period Covered Technical Memorandum
12. Sponsoring Agency Name and Address National Aeronautics and Space Administration, Washington, D.C. 20546		14. Sponsoring Agency Code

15. Supplementary Notes

16. Abstract

A wind tunnel model of an auxiliary inlet ejector with a clamshell flow diverter was evaluated over a range of Mach numbers from 0 to 1.2. Geometric variables included primary nozzle area, shape and position of the auxiliary inlet doors, and the position of the clamshell flow diverter. The efficiency obtained with the doors at a calculated equilibrium position was generally less than the efficiency obtained with the doors at some fixed position. Fixed double-hinge door configurations had higher subsonic-cruise efficiency than fixed single-hinge door configurations. At Mach 0.9, the optimum subsonic-cruise configuration gave an efficiency of 0.902.

17. Key Words (Suggested by Author(s))	18. Distribution Statement
Propulsion Nozzles	Unclassified - unlimited

19. Security Classif. (of this report)	20. Security Classif. (of this page)	21. No. of Pages	22. Price *
Unclassified	Unclassified	41	$3.00

*For sale by the Clearinghouse for Federal Scientific and Technical Information
Springfield, Virginia 22151

PERFORMANCE OF A FIXED GEOMETRY WIND TUNNEL MODEL OF AN AUXILIARY INLET EJECTOR WITH A CLAMSHELL FLOW DIVERTER FROM MACH 0 TO 1.2

by Fred W. Steffen and Albert L. Johns

Lewis Research Center

SUMMARY

A wind tunnel model of an auxiliary inlet ejector with a clamshell flow diverter was evaluated over a range of Mach numbers from 0 to 1.2. Two primary nozzles were used: the smaller one simulated a subsonic-cruise and dry-acceleration primary nozzle position, and the larger one simulated a reheat-acceleration primary nozzle position. Other geometric variables included the shape and position of the auxiliary inlet doors and the position of the clamshell flow diverter.

At subsonic-cruise power settings, fixed double-hinge door configurations gave higher efficiencies than fixed single-hinge door configurations. At Mach 0.9, the double-hinge door configuration had a maximum efficiency of 0.902, and the single-hinge door configuration had a maximum efficiency of 0.882. At other power settings, door shape had little effect on efficiency.

In general, the estimated efficiency which would be obtained if the doors were free to float was less than the maximum which could be obtained if the doors were actuated to the optimum position. In many instances, however, the difference in efficiency was less than 1 percent.

The fixed shroud flap position was the same as that of a floating flap only at a limited combination of power settings and Mach numbers. If the shroud flaps had been free to move, they would have been further open than the flap geometry tested at subsonic-cruise power settings for all Mach numbers tested, at all reheat-acceleration power settings except at $M_0 = 0$ and at $0.85 \leq M_0 \leq 0.95$ with the clamshells at 0°, and at dry-acceleration power settings for $M_0 \geq 0.95$.

With the clamshell flow diverter at the subsonic-cruise position of 17°, pumping characteristics were sufficient to obtain a corrected secondary-weight-flow ratio of 4 percent from a free-stream total-pressure source at all conditions tested except at Mach zero. Moving the clamshell flow diverter to 0° improved the reheat-acceleration nozzle efficiency but significantly reduced the pumping capability.

INTRODUCTION

In its current program in airbreathing propulsion, the Lewis Research Center is evaluating various exhaust nozzle concepts appropriate for supersonic-cruise applications. It is important that these nozzles have good subsonic-cruise and transonic acceleration performance. One such nozzle being considered is the auxiliary ejector. In this nozzle type, auxiliary inlets admit air from the free stream and prevent excessive overexpansion of the primary and secondary streams at low nozzle pressure ratios. Hence, there is a reduced requirement for exit-area variation and a corresponding reduction in projected boattail area at off-design and transonic speeds. If the tertiary flow can be handled efficiently, an overall increase in low-pressure-ratio performance can be realized. The static performance of an auxiliary inlet ejector for supersonic-cruise aircraft is reported in reference 1.

This report presents the isolated performance of a wind tunnel model of an auxiliary inlet ejector with a clamshell flow diverter in the ejector shroud. In the fully open (or supersonic cruise) position, the clamshell is intended to provide a conical expansion surface for efficient high-pressure-ratio operation. In the partly closed (or subsonic cruise) position, the maximum flow area available to the primary jet is reduced, and additional flow area is provided for the tertiary flow around the outside of the clamshell. When rotated to the fully closed position, the clamshell provides the blockage necessary for reverse-thrust operation.

The tests were made using a series of fixed-geometry hardware. Single- and double-hinge auxiliary inlet doors were each tested at four positions, from fully open to fully closed. Two primary nozzles were used; the smaller one simulated a subsonic-cruise and dry-acceleration primary nozzle position, and the larger one simulated a reheat-acceleration primary nozzle position. For closed-door configurations using the small primary nozzle, the clamshells were tested in the fully open position only. For closed-door configurations using the large primary nozzle, the clamshells were used both in the fully open position and a partly closed position. For all open-door configurations, the clamshells were partly closed. The ejector shroud used for all tests simulated a shroud with single-hinge trailing-edge flaps in a closed position.

The tests were conducted in the Lewis Research Center's 8- by 6-Foot Supersonic Wind Tunnel at free-stream Mach numbers from 0 to 1.2 and at nozzle pressure ratios appropriate to the simulated power settings and free-stream Mach number. Room-temperature air was used as the primary and secondary fluid. Nozzle efficiency, pumping characteristics, boattail pressure drag, door-hinge moments, and shroud flap-hinge moments were determined.

APPARATUS

Nozzle

The wind tunnel model of the auxiliary inlet ejector is shown in figure 1. The ejector was assembled from three basic components: a primary nozzle, an auxiliary inlet door section, and a shroud section containing a clamshell flow diverter. These components are shown in figure 2. The stations shown in this and subsequent figures are in terms of inches (cm) from the support model nose. Symbols are defined in appendix A. Also shown in figure 2 are typical static-pressure-tap locations. These pressures were used for the calculation of door-hinge and shroud flap-hinge moments, boattail drag, and door drag.

The primary nozzle, which was modeled from a General Electric J85-GE-13 variable-area primary nozzle, is shown in figure 3. Secondary air was directed through 12 slots in a ring which simulated the primary nozzle actuator blockage. Two different throat areas were used. The smaller throat area corresponded to an area required during subsonic cruise and dry acceleration, while the larger area corresponded to an area required during reheat acceleration.

The auxiliary inlet door section geometry is shown in detail in figure 4. Figure 4(a) shows the single-hinge door geometry, and figure 4(b) shows the double-hinge door geometry. The 16 equally spaced doors were simulated by a continuous circular ring which was divided into doors by 16 equally spaced struts. The space between each strut was 1.3 inches (3.3 cm). Door cross-sectional flow area was considered to be the sum of 16 areas, each 1.3 inches (3.3 cm) in width, with a height measured normal to the door at the trailing edge of the door. For each type of door, four different door positions, from closed to fully open, were tested. By changing the door angle from closed to fully open, door cross-sectional flow area was varied from 0 to 0.56 of the ejector exit area.

The shroud section with the clamshell flow diverter is shown in figure 5. Figure 5(a) shows the clamshell flow diverter in the 0°, or supersonic-cruise, position. In this position, the clamshell formed an integral part of the 9° 7' conical ejector wall and extended from upstream of the secondary throat to the 60° 11' parting line indicated in figure 5(a). Figure 5(b) shows the clamshell flow diverter in the 17°, or subsonic-cruise, position. For closed-door configurations using the small primary nozzle, the diverter was tested at 0° only. For closed-door configurations using the large primary nozzle, the diverter was tested at both 0° and 17°. For all open-door configurations, the diverter was tested at 17° only.

The downstream end of the shroud simulated a section comprised of single-hinge trailing-edge flaps. The fixed-geometry section used during these tests represented a fully closed flap position.

Test Facility and Instrumentation

A schematic view of the wind tunnel support model and instrumentation is shown in figure 6. The cylindrical portion of the model was 8.5 inches (21.6 cm) in diameter. The model mounting strut, which contained the air supply tubes and the instrumentation lines, was 1.75 inches (4.43 cm) thick, with 5° half-angle leading and trailing edges. The boundary-layer characteristics at the aft end of the support model are contained in reference 2. Momentum thickness varied from 0.0221 diameter at Mach 0.56 to 0.0184 diameter at Mach 1.19. A load cell was used to measure the net force on the free parts of the system.

A more detailed view of the instrumentation at the primary nozzle inlet station is shown in figure 7. Typical total-pressure profiles measured at this station are shown in figure 8. The secondary total pressure was measured somewhat further downstream at a station within the simulated primary nozzle actuator mechanism, as indicated in figure 2.

The necessary measurements and equations used to calculate the measured gross thrust minus drag, as well as the ideal gross thrust of a nozzle installed on this support model, are given in reference 3. These equations require a value for the flow coefficient C_D of the primary nozzle. The coefficients for the primary nozzles were obtained from unreported data where flow was measured with a calibrated ASME sharp-edge orifice in the primary air supply line. The flow coefficients obtained in this manner and used to obtain the efficiencies reported herein were 0.977 for the small primary nozzle and 0.985 for the large primary nozzle.

PROCEDURE

Figure 9 is a plot of nozzle pressure ratio P_7/p_0 as a function of flight Mach number, for a typical supersonic-cruise turbojet nozzle installation. This schedule was used as a guide for setting pressure ratio over the range of Mach numbers from 0 to 1.2 for each power setting. At each Mach number, data were taken at several pressure ratios around the values shown in figure 9 at a nominal value of corrected secondary-weight-flow ratio. Also, at the particular pressure ratio shown in figure 9 for a Mach number and power setting, data were taken over a range of corrected

secondary-weight-flow ratios from 0 to 0.15. The basic data, consisting of gross-thrust coefficients and pumping characteristics, are presented in appendix B. These data were used in conjunction with the pressure ratio - Mach number schedule of figure 9 to present the nozzle performance in the following section.

RESULTS AND DISCUSSION

Single- and Double-Hinge Door Comparison

The maximum nozzle efficiencies obtained with the single- and double-hinge door configurations are shown in figure 10 as a function of free-stream Mach number. The double-hinge door configuration was more efficient at subsonic-cruise power settings (fig. 10(a)), particularly at Mach numbers of 0.85 and 0.9. At Mach 0.9, the double-hinge door configuration had an efficiency of 0.902, as opposed to 0.882 for the single-hinge door configuration. At dry-acceleration power settings (fig. 10(b)), there was little effect of door shape on nozzle efficiency. At Mach 0.9, the double-hinge door configuration had an efficiency of 0.932, and the single-hinge door configuration an efficiency of 0.924. At reheat-acceleration power settings (fig. 10(c)), there was again little effect of door shape on nozzle efficiency. At reheat-acceleration power settings above Mach 0.85, the maximum efficiency was obtained with closed doors (so that door shape was unimportant) and with the clamshell flow diverter set at 0°. Moving the clamshell flow diverter from 17° to 0° increased the efficiency from 0.922 to 0.944 at Mach 1.0.

Maximum and Equilibrium Door Performance

In figures 11(a) to (c), the performance obtained with the single-hinge doors set at the maximum efficiency position is compared to the interpolated performance obtained with the single-hinge doors at a calculated floating equilibrium position. Nozzle efficiency, door position, and the required ratio of secondary total pressure to free-stream total pressure for the specified corrected secondary-weight-flow ratio are presented as a function of free-stream Mach number.

Figure 11(a-1) shows the subsonic-cruise nozzle efficiency with the doors in the equilibrium position to be only slightly less than maximum between Mach numbers of 0.85 and 0.95. The equilibrium door angle (fig. 11(a-2)) was less (more closed) than the door angle for maximum efficiency. Comparison of the P_s/P_0 curves for the ejector (fig. 11(a-3)) with a curve of p_0/P_0 shows that P_s is approximately equal to p_0

as a result of the open doors. The tailed symbols and curves in this and subsequent figures signify that the limited static-pressure instrumentation indicated that an opening moment was acting on the shroud flaps. Thus, the equilibrium position of the doors might be different if the flaps were capable of moving to their equilibrium position.

Figure 11(b) shows the dry-acceleration performance of the ejector with the single-hinge doors. Between Mach numbers of 0.7 and 0.9, the nozzle efficiency (fig. 11(b-1)) with the doors in the calculated equilibrium position was only slightly less than maximum (0.8 percent at Mach 0.85). The equilibrium position of the door (fig. 11(a-2)) was equal to or less than the door position for maximum efficiency. At Mach numbers of 0, 0.9, and 0.95, the equilibrium door position resulted in maximum efficiency. At Mach 0, the secondary total pressure required to obtain a 4-percent corrected secondary-weight-flow ratio $\omega\sqrt{\tau}$ (fig. 11(b-3)) exceeded the ambient pressure. At Mach numbers from 0.6 to 1.0, secondary pressure recoveries from 0.86 to 0.66 were required for $\omega\sqrt{\tau} = 0.04$. Secondary total pressures required for $\omega\sqrt{\tau} = 0.04$ were greater than p_0. Below Mach 0.95, the shroud flaps would have been in the position tested (assuming this to be the inner-stop position).

The reheat-acceleration performance of the ejector with the single-hinge doors is shown in figure 11(c). From Mach 0.7 to 0.85, the nozzle efficiency with the doors in an equilibrium position (fig. 11(c-1)) was essentially equal to the maximum efficiency, even though the difference in door position was as much as 10° (fig. 11(c-2)). Above Mach 0.85, the clamshell must be set at 0° to obtain maximum efficiency. However, the required secondary total-pressure recovery for 4-percent corrected secondary-weight-flow ratio exceeded 100 percent when this was done. This was aggravated by the increase in ejector spacing ratio at reheat conditions, which was required to simulate a translating iris primary nozzle. Other data at Mach 1.2 indicated that a corrected secondary-weight-flow ratio of 0.02 could be obtained with a recovery of 82 percent and the reduction in efficiency would amount to only 0.3 percent.

For most of the data shown in figure 11(c), an opening moment acts on the shroud flap. Thus, it should again be recognized that the equilibrium door position might be different if the flaps were capable of moving to an equilibrium position.

Figures 12(a) to (c) show the performance of the ejector with double-hinge doors. The method of estimating the floating position of these double-hinge doors is given in appendix C. Again, performance with the doors set at the maximum efficiency position is compared to the performance with the doors at the estimated equilibrium position. At subsonic cruise (fig. 12(a)), there was a larger difference between maximum efficiency and equilibrium efficiency than there was for the single-hinge doors at Mach numbers of 0.85 and 0.90. Otherwise, the double-hinge door performance exhibited the same general trends as the single-hinge door performance.

A general trend noted in figures 11 and 12 is that with the doors in the position for maximum efficiency, the secondary total pressure was equal to or greater than the secondary total pressure with the doors in an equilibrium position. This indicate that part of the improvement in nozzle efficiency resulted from increased pressures in the primary nozzle base region.

Performance Variation With Door Angle and Secondary Flow

Some typical effects of auxiliary inlet door angle for both single- and double-hinge configurations are shown in figures 13 and 14. The nozzle efficiencies were generally more sensitive to door-angle variations when the nozzle flow tended to be most overexpanded (subsonic-cruise or dry-acceleration power settings at low Mach numbers, figs. 13(a) and (b), and 14(a) and (b)) and when the nozzle flow was almost fully expanded (reheat-acceleration power setting at Mach 1.2, figs. 13(c) and 14(c)). The ratio of secondary total pressure to free-stream total pressure required for a specified corrected secondary-weight-flow ratio was rather insensitive to, but generally increased with, door angle. An exception to this general trend occurred with a reheat-acceleration power setting at the higher nozzle pressure ratios. At these conditions (when the primary flow is almost fully expanded and pressure forces would tend to close the doors), opening the doors may provide an overboard flow path for the secondary flow and thus reduce the secondary pressures with an accompanying loss in performance.

The effect of corrected secondary-weight-flow ratio on nozzle performance is shown in figure 15(a) for single-hinge doors and in figure 15(b) for double-hinge doors. The data are shown for typical open-door configurations at Mach 0.9 at two levels of pressure ratio. At the lower (subsonic cruise) pressure ratio, where the nozzle was more overexpanded, the efficiency dropped sharply for secondary flow ratios less than 0.05. Peak efficiency occurred at a corrected secondary-weight-flow ratio of about 0.10. A ratio of secondary total pressure to free-stream total pressure of 0.7 would be required to supply the secondary flow. At the higher (dry acceleration) pressure ratio, the efficiency was less sensitive to corrected secondary-weight-flow ratio. The efficiency reached a value close to maximum at a corrected secondary-weight-flow ratio of about 0.04. A ratio of secondary total pressure to free-stream total pressure of 0.7 was required to supply the secondary flow. It should be pointed out that the flat efficiency curve is probably characteristic only of a fixed open-door configuration and that the efficiency might be more sensitive to secondary flow if the door were less open or free to float.

The door-hinge moment coefficients per inch of hinge are shown in figure 16(a) as a function of door angle for the single-hinge doors. These curves were used to

estimate the equilibrium position of the single-hinge doors. The data were obtained from a single row of static-pressure taps on the outer surface of a door at $\theta = 157.5^{\circ}$ and from a single row of static-pressure taps on the internal surface of a door at $\theta = 0^{\circ}$. Thus, the instrumented doors were close to the hubs of the clamshells and may not be representative of all doors around the circumference. For subsonic cruise and dry acceleration (figs. 16(a-1) and (a-2)), the curves generally have negative slopes, indicating that the doors were statically stable. Stable equilibrium would occur at the door angles at which the curves cross the abscissa (i.e., $C_m = 0$). For reheat acceleration (fig. 16(a-3)) at Mach numbers above 0.7 and with the clamshells at 17°, the moment coefficient curves have positive slopes below door angles of 10°, thereby indicating static instability. Also, the moment coefficients were negative for all door positions. Thus, during reheat acceleration, the doors would close at a Mach number between 0.7 and 0.85 and would stay closed at higher Mach numbers. It is also shown that with the doors at 0°, moving the clamshells from 17° to 0° causes a greater negative door moment.

The hinge-moment coefficients for the double-hinge doors are shown in figure 16(b). Hinge-moment coefficients about the upstream hinge are presented. The assumed mechanism and the equations used to obtain the moments about the upstream hinge are explained in appendix C. The double-hinge doors appeared to behave in the same manner as the single-hinge doors except that at reheat acceleration (fig. 16(b-3)) the doors would close at a lower Mach number, between 0.6 and 0.7.

Pressure Drag

The boattail pressure drag is shown for the single-hinge door configuration in figure 17(a) and for the double-hinge door configurations in figure 17(b). The boattail pressure drag was obtained from a single row of 10 static-pressure taps located behind a door at $\theta = 180^{\circ}$. These figures show that boattail drag was a significant percentage of ideal thrust at subsonic-cruise Mach numbers of 0.7, 0.85, and 0.9 only when the doors were closed. With the doors in their normally open subsonic-cruise position, the boattail drag almost disappears. High boattail pressure drags are shown at other power settings at Mach numbers of 0.95 and greater because of the closed trailing-edge flap section used on all the configurations.

The boattail pressure drag is compared to the pressure drag from the external surface of the auxiliary inlet doors in figure 18. The comparison is made at a subsonic-cruise power setting and Mach 0.9. For the single-hinge doors (fig. 18(a)), the pressure drag of the doors was greater than from the 9° 34' boattail, particularly at a door angle of 20°. For the double-hinge doors (fig. 18(b)), the pressure drag of the doors was slightly less than that from the boattail.

SUMMARY OF RESULTS

A fixed-geometry wind tunnel model of an auxiliary inlet ejector with a clamshell flow diverter was evaluated over a range of Mach numbers from 0 to 1.2. Two primary nozzles were used: the smaller one simulated a subsonic-cruise and dry-acceleration primary nozzle position, and the larger one simulated a reheat-acceleration primary nozzle position. Other geometric variables included the shape and position of the auxiliary inlet doors and the position of the clamshell flow diverter. Room-temperature air was used as the primary and secondary fluid. Nozzle efficiency, gross-thrust coefficients, pumping characteristics, boattail pressure drag, door-hinge moments, and shroud flap-hinge moments were determined. The results were as follows:

1. At subsonic-cruise power settings, with the clamshell flow diverted at 17°, the double-hinge door configurations had higher maximum efficiency. At Mach 0.9, the double-hinge door configuration had a maximum efficiency of 0.902, and the single-hinge door configuration had a maximum efficiency of 0.882.

2. At dry-acceleration power settings, with the clamshell flow diverter at 17°, the nozzle efficiencies of the double- and single-hinge door configurations were nearly equal. At Mach 0.9, the double-hinge door configuration had a maximum efficiency of 0.932, and the single-hinge door configuration had a maximum efficiency of 0.924.

3. At reheat-acceleration power settings, with the clamshell flow diverter at 17°, there was little difference in nozzle efficiency between the double- and single-hinge door configurations. Above Mach 0.85, the optimum door position was closed, and thus door shape would not affect nozzle efficiency. The lowest value of efficiency was 0.944, occurring at Mach 1.0.

4. At reheat-acceleration power settings, moving the clamshell from 17° to 0° with the doors closed improved the efficiency. At Mach 1.2, the efficiency increased from 0.917 to 0.950.

5. Except at a free-stream Mach number of 0, all configurations tested with the clamshell at 17° appeared to be able to pump at least 4-percent corrected secondary flow from a free-stream source at all power settings. However, at a reheat-acceleration power setting with the clamshell at 0° and the doors closed, only about 2-percent corrected secondary flow could be obtained from a free-stream source. If such a reduction in cooling flow could be tolerated, the efficiency would be reduced by only 0.3 percent.

6. With the shroud flap fixed in the position tested, the equilibrium position of the doors was generally not the position for maximum performance. With the single-hinge door configurations, for example, this difference in nozzle efficiency was 0.8 percent at a Mach number of 0.85 for both subsonic-cruise and dry-acceleration power settings.

7. If the shroud flaps had been free to move, they would have been further open at subsonic-cruise and reheat-acceleration power settings. At dry-acceleration power settings, up to Mach 0.95, the flaps would have been closed against inner stops at the fixed-flap position.

8. The doors, both single and double hinge, appeared to be statically stable during subsonic cruise and dry acceleration. During reheat acceleration, at Mach numbers above 0.7, the doors appeared to be statically unstable between door angles of 0° and and 10°.

9. Opening the doors significantly reduced the subsonic-cruise boattail drag at Mach numbers of 0.7, 0.85, and 0.9.

10. With a subsonic-cruise power setting at Mach 0.9, the pressure drag loss of the single-hinge doors was greater than the boattail pressure drag loss. At the same conditions, the pressure drag loss of the double-hinge doors was slightly less than the boattail pressure drag loss.

Lewis Research Center,
National Aeronautics and Space Administration,
Cleveland, Ohio, March 5, 1970,
126-15.

APPENDIX A

SYMBOLS

A	area
A_{max}	simulated nacelle area
C_D	primary nozzle flow coefficient
$(C_m)_\delta$	door-hinge moment coefficient per inch of hinge, $m/(A_{max})(d_{max}/2)(P_7)$
D	drag
D_P	pressure drag
d	diameter
d_{max}	model diameter (equivalent to simulated nacelle diameter)
d_E	shroud-exit diameter
d_p	primary nozzle diameter
d_s	internal shroud diameter
F	jet thrust
$F_1, \ldots, F_4$	forces acting on door
L	ejector shroud length
l	length
M	Mach number
m	moment
P	total pressure
p	static pressure
R	total radius
r	local radius
T	total temperature
W	weight-flow rate
α	flap angle
β	boattail angle
δ_1, δ_2	door angles
θ	angular coordinate, measured clockwise from the top while looking upstream
τ	temperature ratio, T_s/T_p
ω	weight-flow ratio, W_s/W_p

Subscripts:

E	exit
i	ideal
l	local
p	primary
s	secondary station within simulated actuator mechanism
0	free stream
7	inlet to primary nozzle

APPENDIX B

BASIC PERFORMANCE DATA

The basic performance data for all configurations are presented as a function of nozzle pressure ratio in figure 19. Nozzle gross-thrust coefficient and secondary- to primary-total-pressure ratios are presented for a nominal value of corrected secondary-weight-flow ratio. The basic performance data for the closed-door configurations are shown as a function of corrected secondary-weight-flow ratio in figure 20. Nozzle gross-thrust coefficient and secondary- to primary-total-pressure ratio are presented for values of Mach number and pressure ratio as obtained from figure 9.

APPENDIX C

DOUBLE-HINGE DOOR HINGE-MOMENT ANALYSIS

To obtain the hinge moment about the upstream hinge of a double-hinge door, the fixed door was assumed to have the mechanism shown in figure 21. This mechanism, with $l_4 = 2l_6$ would give a door-angle ratio δ_1/δ_2 of approximately 2.0.

Considering the downstream door as a free body in equilibrium, the sum of the forces and moments about X would be equal to 0. The equations to determine the total hinge moment at Z are as follows:

$$F_1 l_1 - F_2 l_2 = 0 \tag{C1}$$

$$F_1 \sin \delta_2 + F_2 \sin \varphi_2 - F_3 \sin \varphi_1 = 0 \tag{C2}$$

$$F_1 \cos \delta_2 + F_2 \cos \varphi_2 - F_3 \cos \varphi_1 = 0 \tag{C3}$$

In these equations, F_3 is considered as the equilibrant; δ_2, φ_2, and l_2 are known constants for any particular door setting; F_1 and l_1 are determined from integrations of measured pressure distributions on the inner and outer surfaces of the rear door; F_2 is the reaction of the pin Y against the side of the slot and must be normal to the side of the slot; F_2, φ_3, and F_3 can be determined from the solution of equation (C1) and the simultaneous solution of equations (C2) and (C3), and

$$F_2 = \frac{F_1 l_1}{l_2} \tag{C4}$$

$$\varphi_1 = \tan^{-1} \frac{F_1 \sin \delta_2 + F_2 \sin \varphi_2}{F_1 \cos \delta_2 + F_2 \cos \varphi_2} \tag{C5}$$

$$F_3 = \frac{F_1 \sin \delta_2 + F_2 \sin \varphi_2}{\sin \varphi_1} \tag{C6}$$

Then the moment about Z due to the forces on the rear door is

$$m_{F\text{-}R} = F_3 l_3 = F_3 l_4 \cos \varphi_3 = F_3 l_4 \cos(\varphi_1 - \delta_2) \tag{C7}$$

where F_3 is the resultant of F_1 and F_2, and δ_2 and l_4 are known constants for any particular door setting. The total moment about Z is then

$$m_Z = m_{F\text{-}R} + F_4 l_5 \tag{C8}$$

where F_4 and l_5 are obtained from integrations of measured pressure distribution on the inner and outer surfaces of the upstream door.

REFERENCES

1. Shrewsbury, George D.; and Jones, John R.: Static Performance of an Auxiliary Inlet Ejector Nozzle for Supersonic-Cruise Aircraft. NASA TM X-1653, 1968.

2. Harrington, Douglas E.: Jet Effects on Boattail Pressure Drag of Isolated Ejector Nozzles at Mach Numbers From 0.60 to 1.47. NASA TM X-1785, 1969.

3. Steffen, Fred W.; and Jones, John R.: Performance of a Wind Tunnel Model of an Aerodynamically Positioned Variable Flap Ejector at Mach Numbers From 0 to 2.0. NASA TM X-1639, 1968.

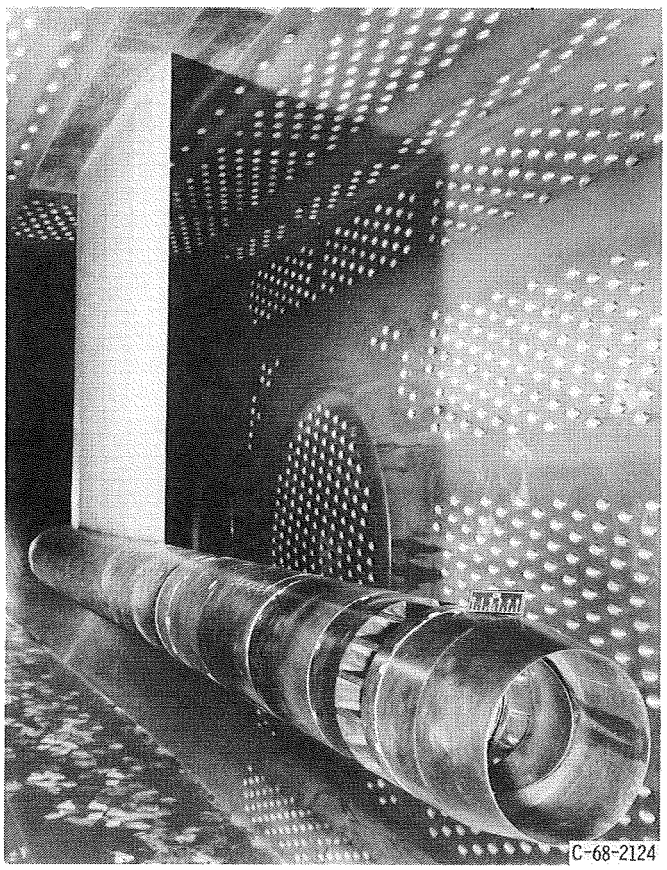

Figure 1. - Auxiliary inlet ejector with clamshell flow diverter installed on wind tunnel support model.

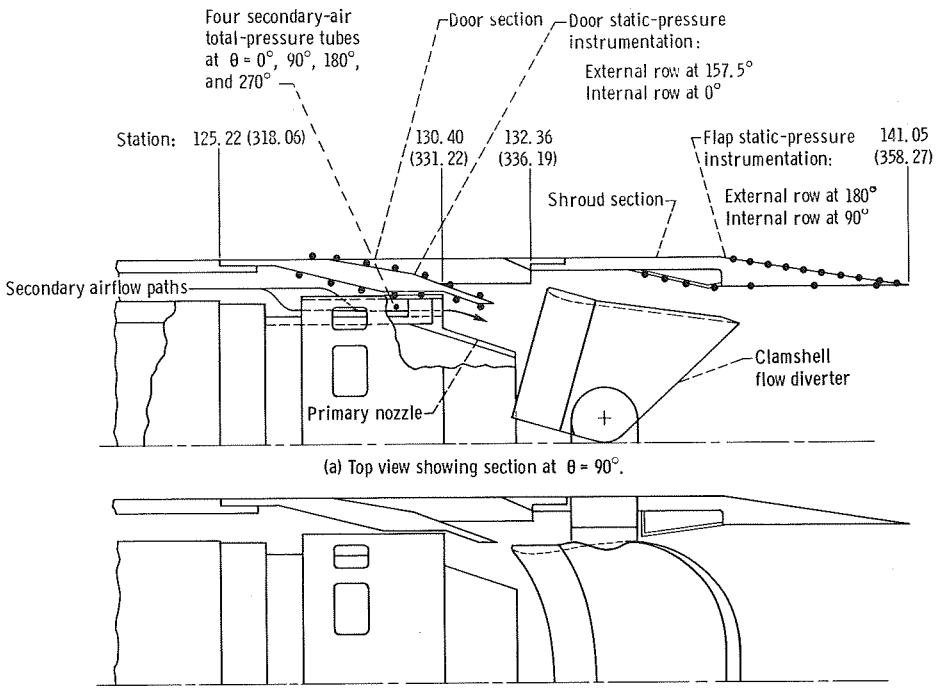

(a) Top view showing section at θ = 90°.

(b) Side view showing section at θ = 0°.

Figure 2. - Auxiliary inlet ejector with clamshell flow diverter. (Stations are in inches (cm).)

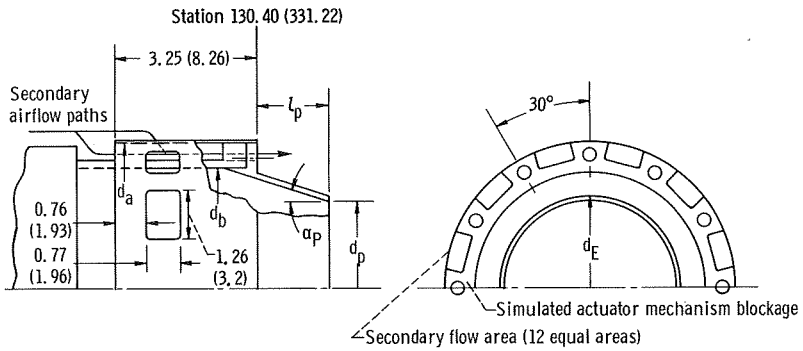

Primary nozzle configuration	Primary nozzle length ratio, ℓ_p/d_{max}	Primary nozzle diameter ratio, d_p/d_{max}	Primary nozzle flap angle, α_P, deg	Diameter ratios			Primary nozzle flow coefficient, C_D
				d_a/d_{max}	d_b/d_{max}	d_E/d_{max}	
Subsonic cruise and dry acceleration	0.18	0.52	13.25	0.79	0.65	0.55	0.977
Reheat acceleration	0.13	0.62	5.30	0.79	0.65	0.64	0.985

Figure 3. - Details of simulated J85-GE-13 primary nozzle. (Station and dimensions are in inches (cm).)

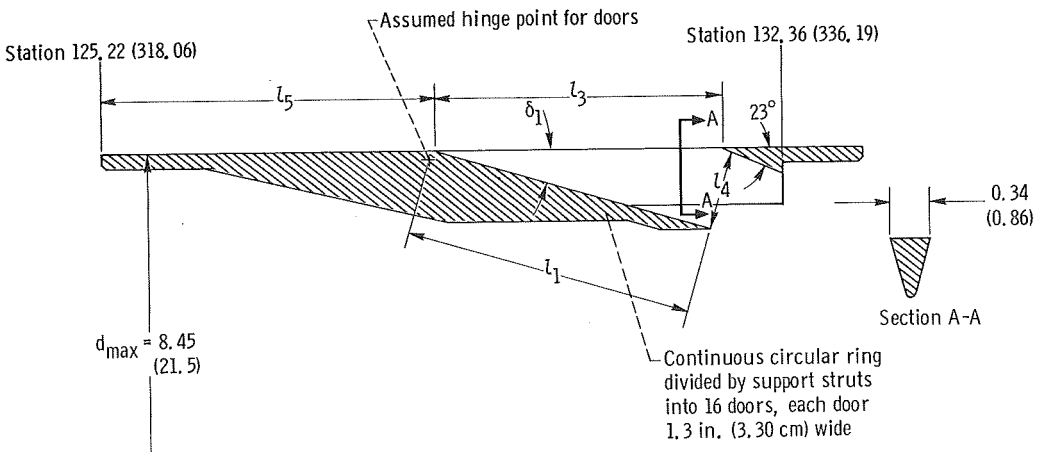

Door angle, δ_1, deg	l_1/d_{max}	l_3/d_{max}	l_4/d_{max}	l_5/d_{max}	$\frac{l_4 \times 1.3 \times 16}{A_E}$
0	0.353	0.353	0	0.406	0
10	.345	.352	.062	.412	.28
16	.353	.358	.101	.406	.46
20	.353	.359	.124	.405	.56

(a) Single-hinge doors.

Figure 4. - Door geometry. (Stations and dimensions are in inches (cm).)

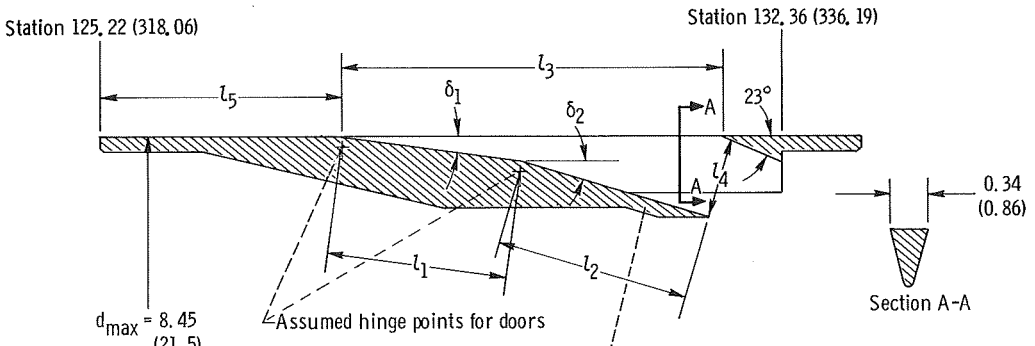

Door angle, deg		l_1/d_{max}	l_2/d_{max}	l_3/d_{max}	l_4/d_{max}	l_5/d_{max}	$\frac{l_4 \times 1.3 \times 16}{A_E}$
δ_1	δ_2						
0	0	0.221	0.240	0.472	0	0.295	0
5	10	.207	↓	.458	.064	.308	.29
8	16	.221		.472	.097	.295	.44
10	20	.225		.473	.122	.291	.55

(b) Double-hinge doors.

Figure 4. - Concluded.

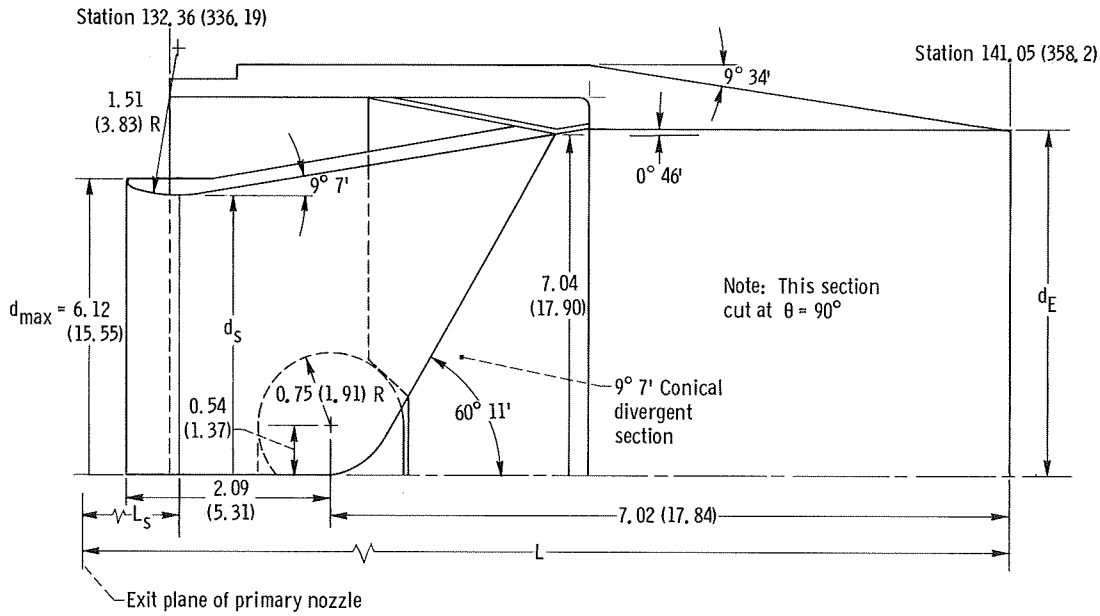

Primary nozzle configuration	d_E/d_p	d_s/d_p	L_s/d_p	L/d_p	d_E/d_{max}
Subsonic cruise and dry acceleration	1.602	1.33	0.137	2.065	0.833
Reheat acceleration	1.357	1.12	0.173	1.828	0.833

(a) Clamshell at 0°.

Figure 5. - Shroud and clamshell flow diverter geometry. (Stations and dimensions are in inches (cm).)

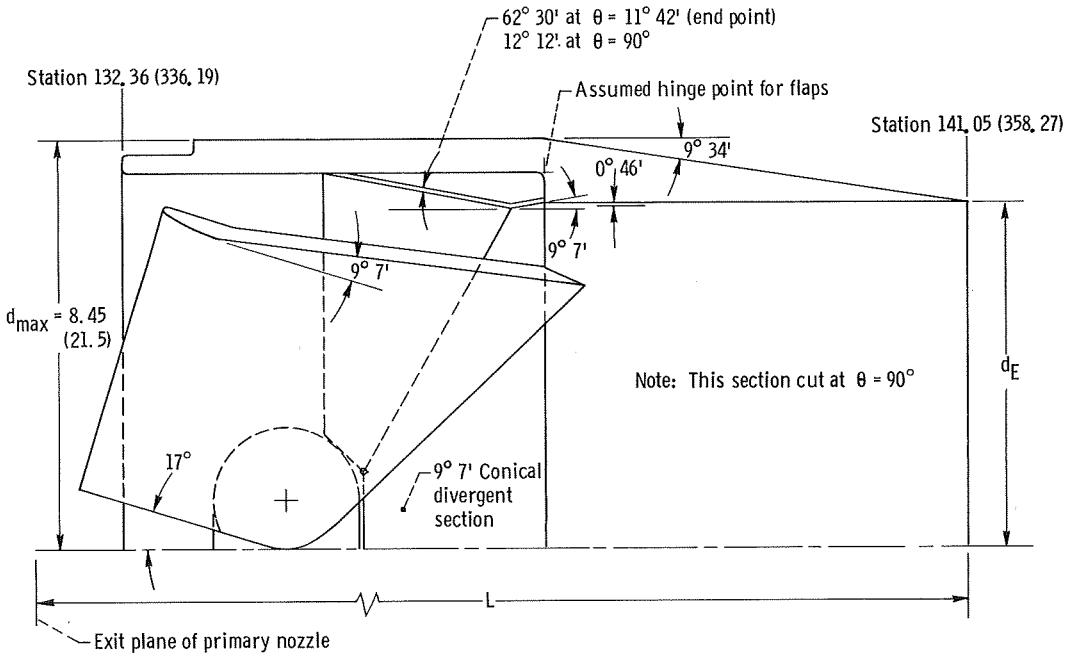

Primary nozzle configuration	d_E/d_p	L/d_p	d_E/d_{max}
Subsonic cruise and dry acceleration	1.602	2.065	0.833
Reheat acceleration	1.357	1.828	0.833

(b) Clamshell at 17°.

Figure 5. - Concluded.

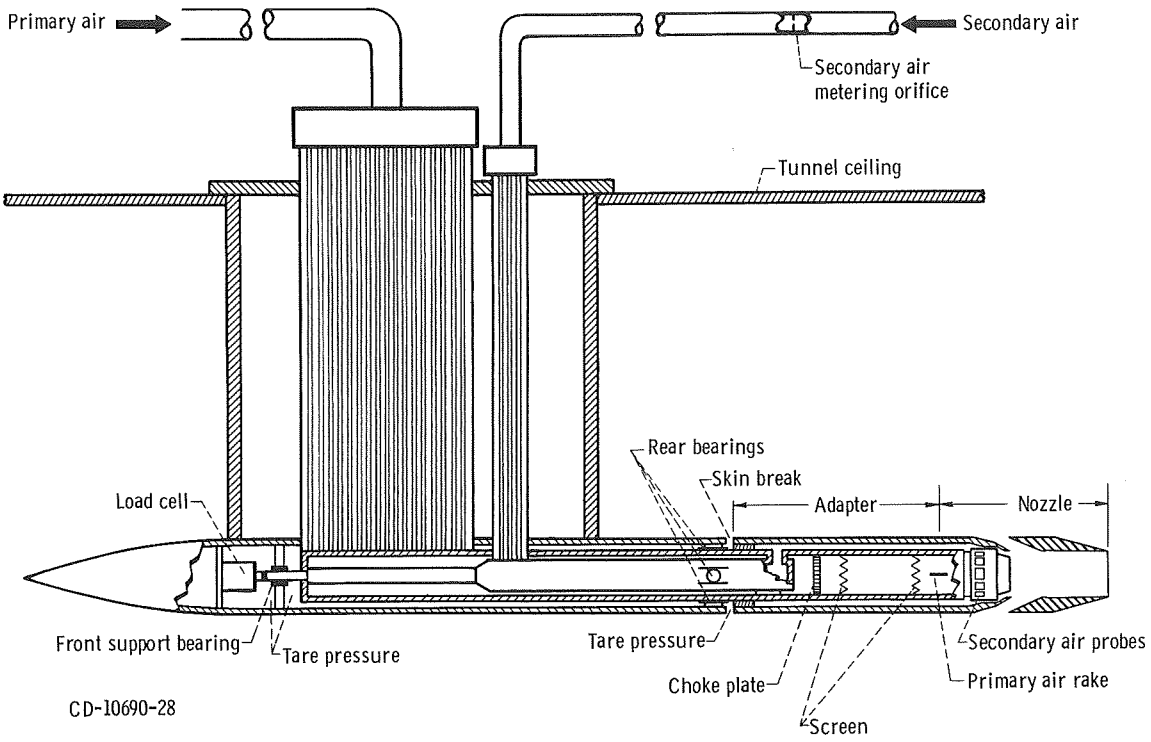

Figure 6. - Schematic view of nozzle support model and air supply system.

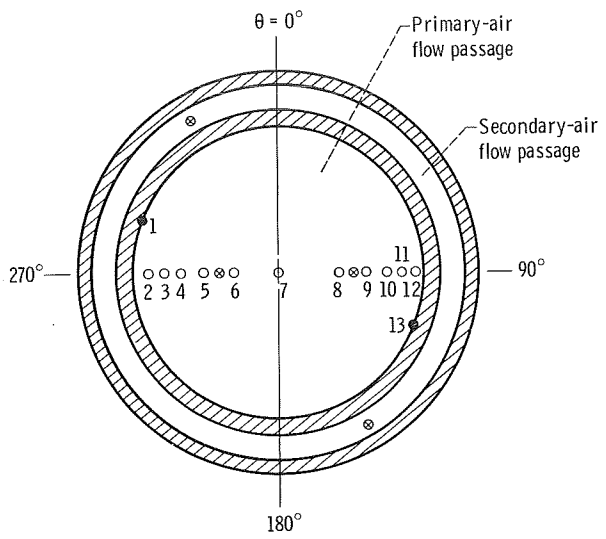

Primary flow orifice	Normalized distance from centerline, r/R
1	1.000
2	.900
3	.790
4	.670
5	.519
6	.300
7	0
8	-.418
9	-.600
10	-.750
11	-.855
12	-.950
13	-1.000

Figure 7. - Details of instrumentation at station 7. Total radius, R = 3.006 inches (7.635 cm).

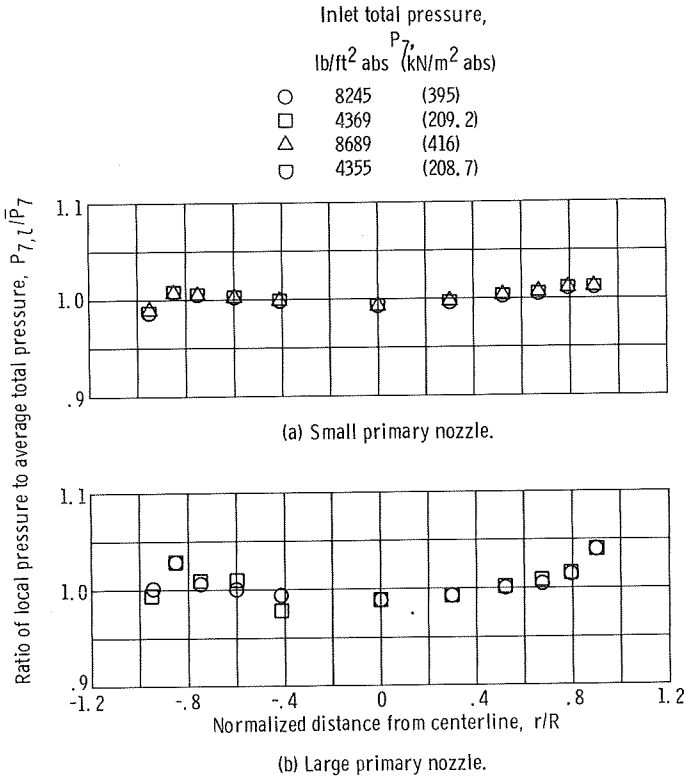

Figure 8. - Total-pressure profile at primary nozzle inlet (station 7.)

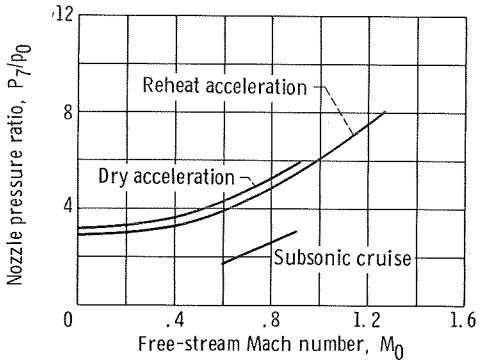

Figure 9. - Schedule of nozzle pressure ratio with free-stream Mach number.

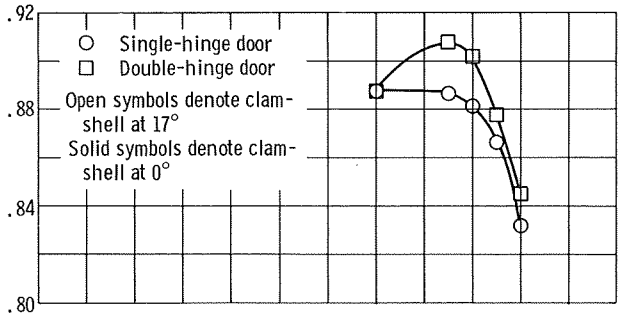

(a) Subsonic cruise.

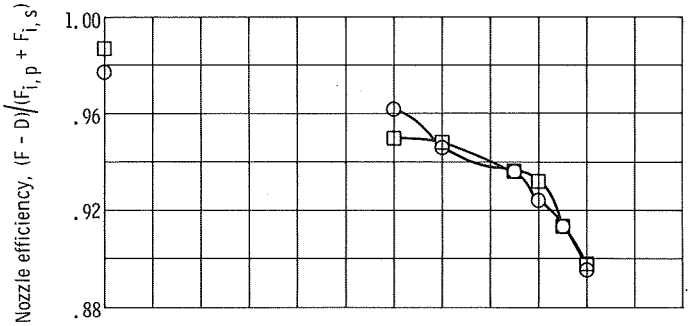

(b) Dry acceleration.

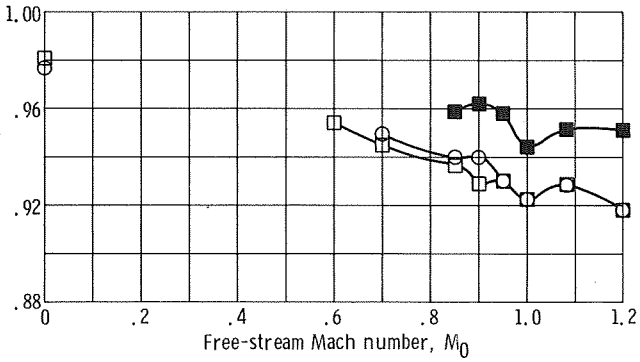

(c) Reheat acceleration.

Figure 10. - Effect of door shape on maximum nozzle efficiency. Corrected secondary-weight-flow ratio, $\omega\sqrt{\tau} = 0.04$.

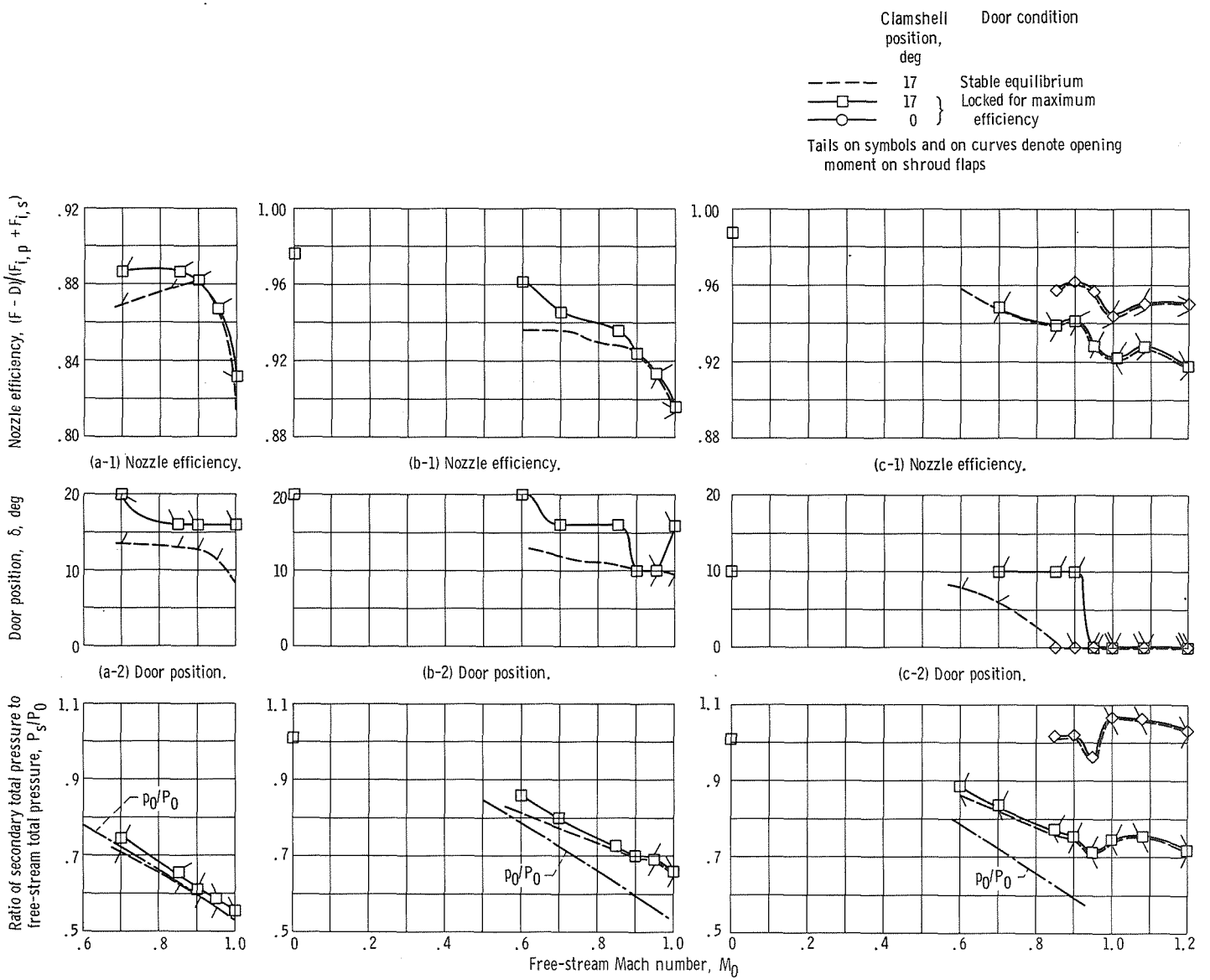

Figure 11. - Performance of ejector with single-hinge doors. Corrected secondary-weight-flow ratio, $\omega\sqrt{\tau} = 0.04$. Clamshell position, 17°.

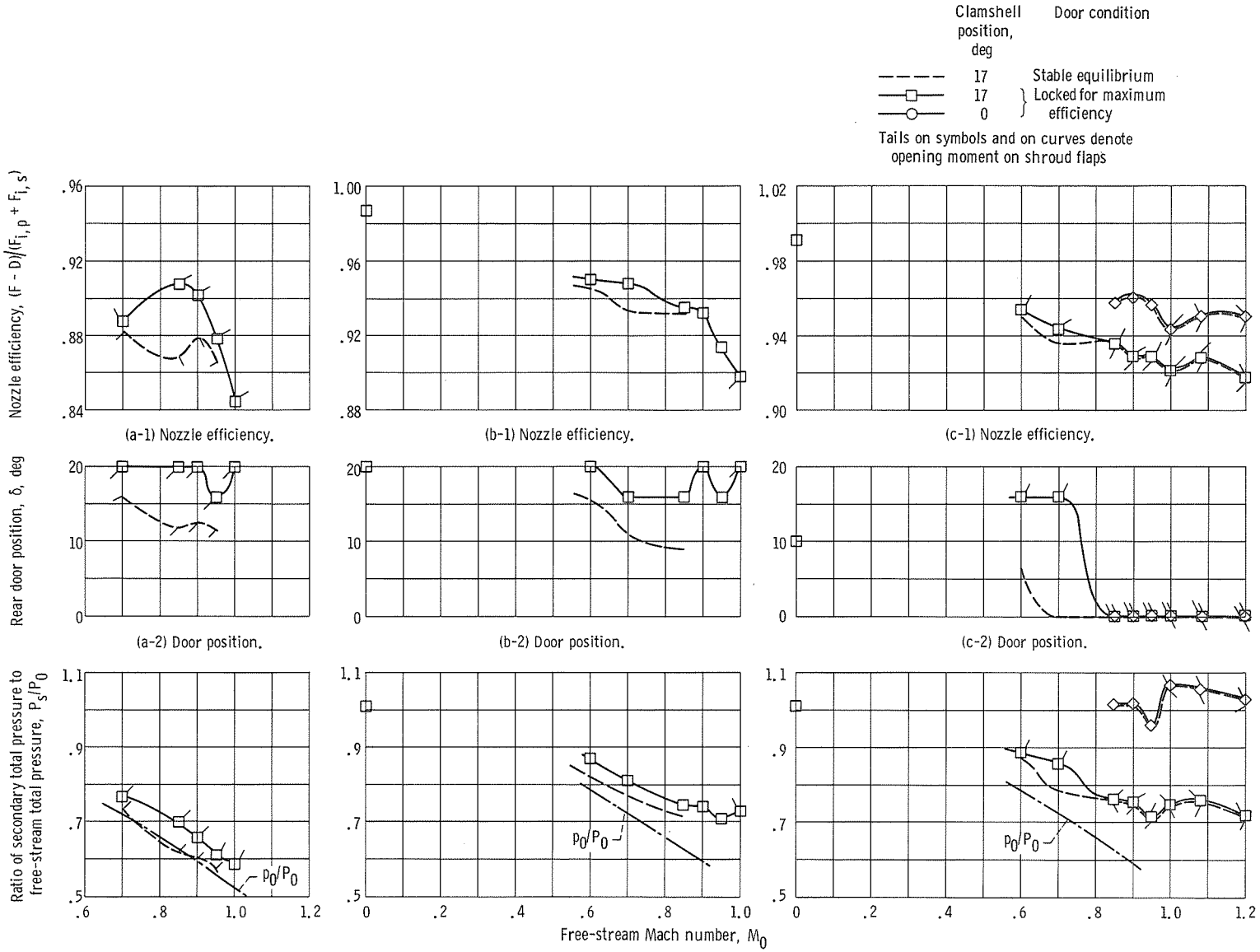

(a-1) Nozzle efficiency.

(b-1) Nozzle efficiency.

(c-1) Nozzle efficiency.

(a-2) Door position.

(b-2) Door position.

(c-2) Door position.

(a-3) Total-pressure ratio.

(b-3) Total-pressure ratio.

(c-3) Total-pressure ratio.

(a) Subsonic-cruise performance.

(b) Dry-acceleration performance.

(c) Reheat-acceleration performance.

Figure 12. - Performance of ejector with double-hinge doors. Corrected secondary-weight-flow ratio, $\omega\sqrt{\tau} = 0.04$.

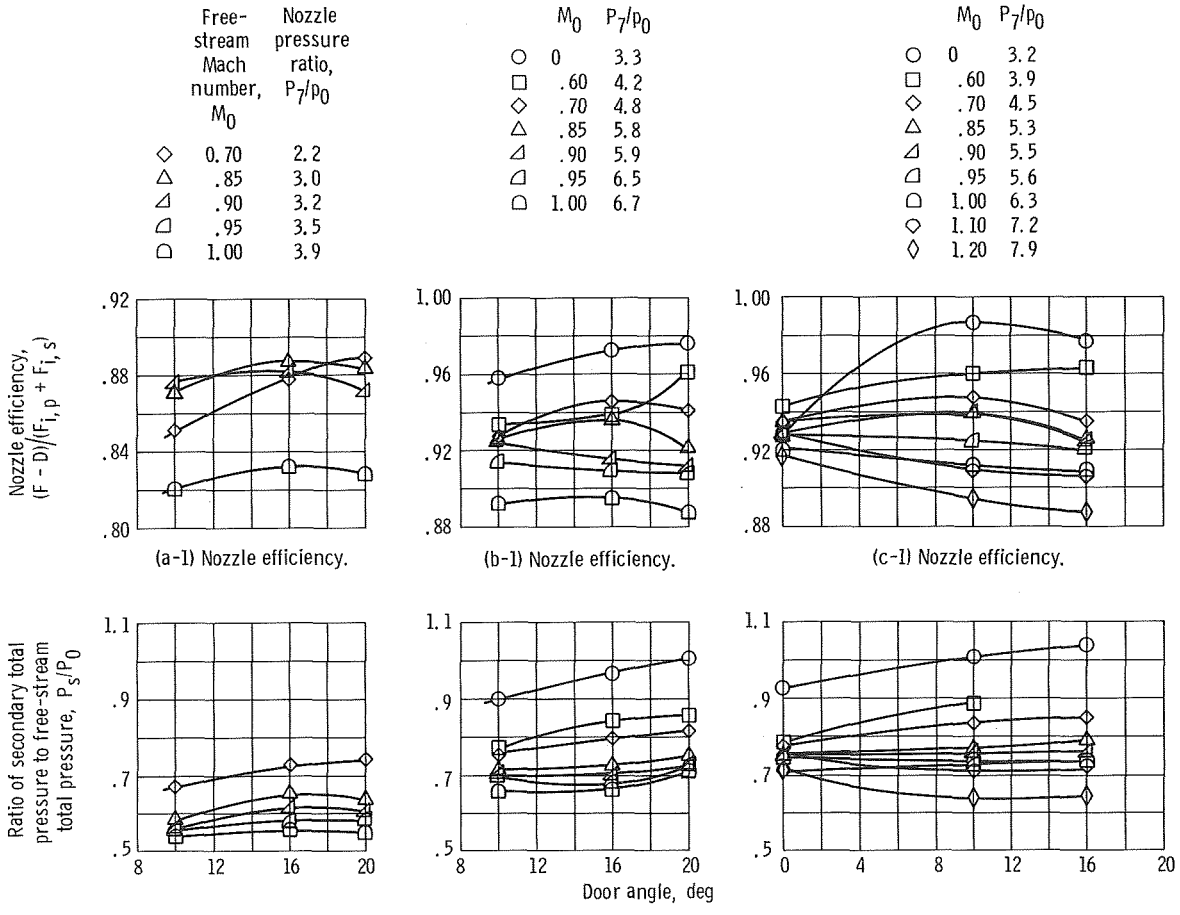

(a-1) Nozzle efficiency.

(b-1) Nozzle efficiency.

(c-1) Nozzle efficiency.

(a-2) Total-pressure ratio.

(b-2) Total-pressure ratio.

(c-2) Total-pressure ratio.

(a) Subsonic-cruise performance.

(b) Dry-acceleration performance.

(c) Reheat-acceleration performance.

Figure 13. - Effect of door position on performance of ejector with single-hinge doors. Clamshell at 17°; corrected secondary-weight-flow ratio, $\omega\sqrt{\tau} = 0.04$.

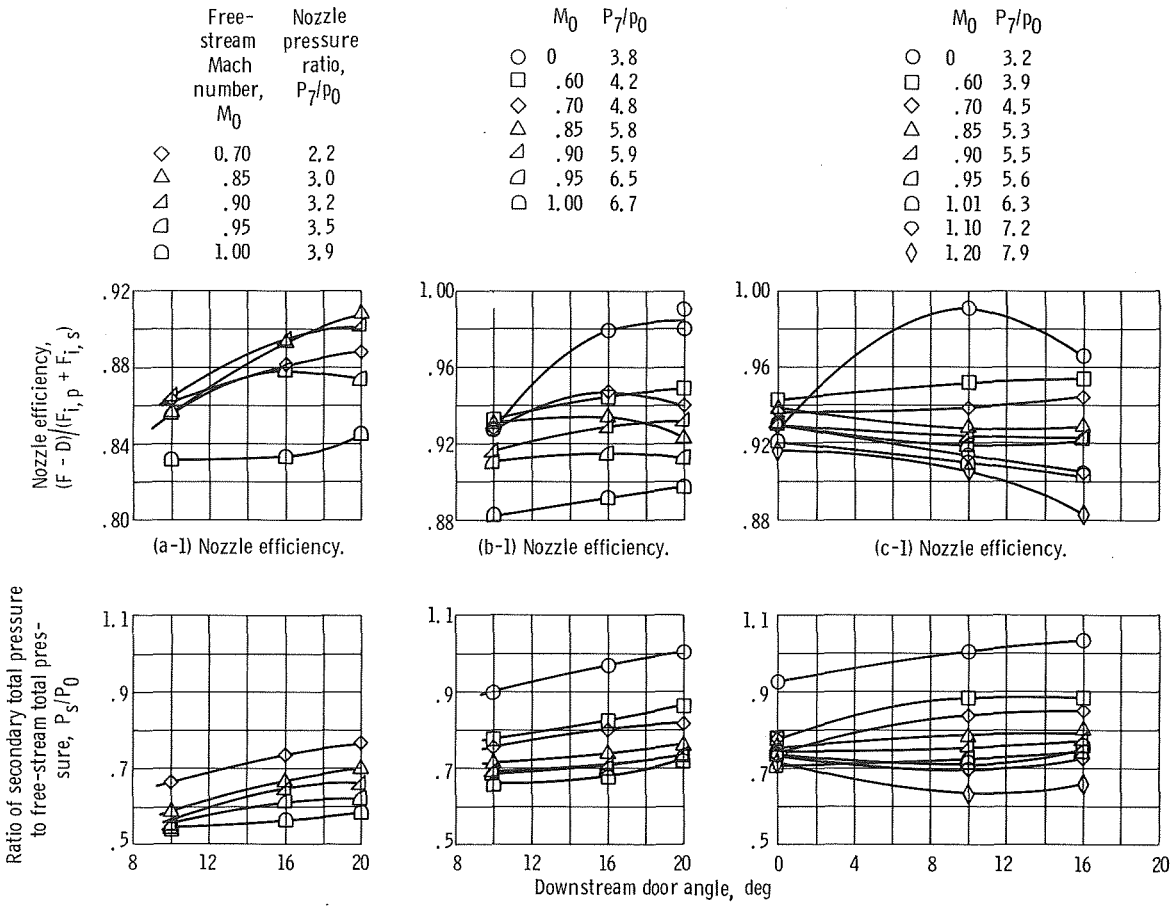

(a-1) Nozzle efficiency.

(b-1) Nozzle efficiency.

(c-1) Nozzle efficiency.

(a-2) Total-pressure ratio.

(b-2) Total-pressure ratio.

(c-2) Total-pressure ratio.

(a) Subsonic-cruise performance.

(b) Dry-acceleration performance.

(c) Reheat-acceleration performance.

Figure 14. - Effect of door position on performance of ejector with double-hinge doors. Clamshell at 17°; corrected secondary-weight-flow ratio, $\omega\sqrt{\tau} = 0.04$.

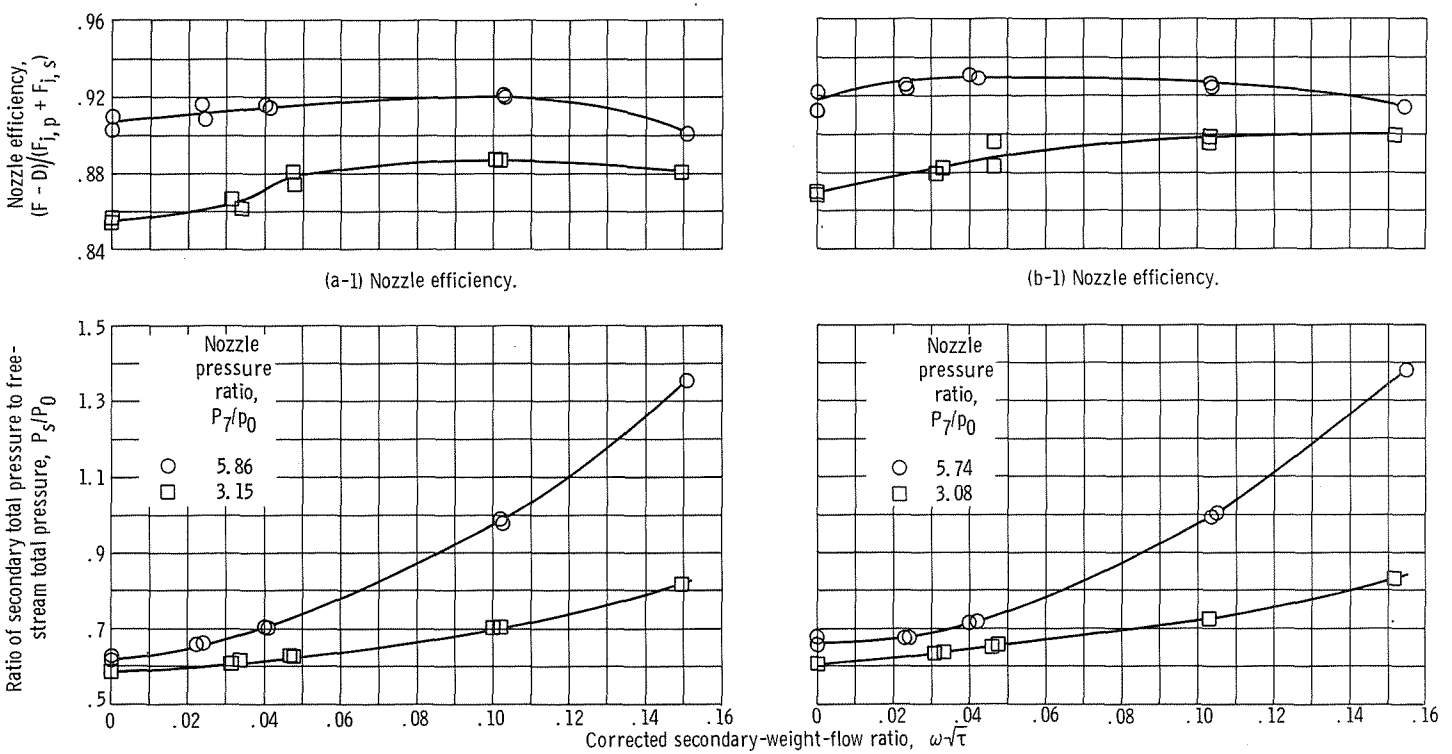

(a-1) Nozzle efficiency.

(b-1) Nozzle efficiency.

(a-2) Total-pressure ratio.

(b-2) Total-pressure ratio.

(a) Single-hinge door. Door angle, 16°.

(b) Double-hinge door. Downstream door angle, 16°.

Figure 15. - Effect of corrected secondary-weight-flow ratio on performance of typical single- and double-hinge open-door configurations at Mach 0.90. Small primary nozzle.

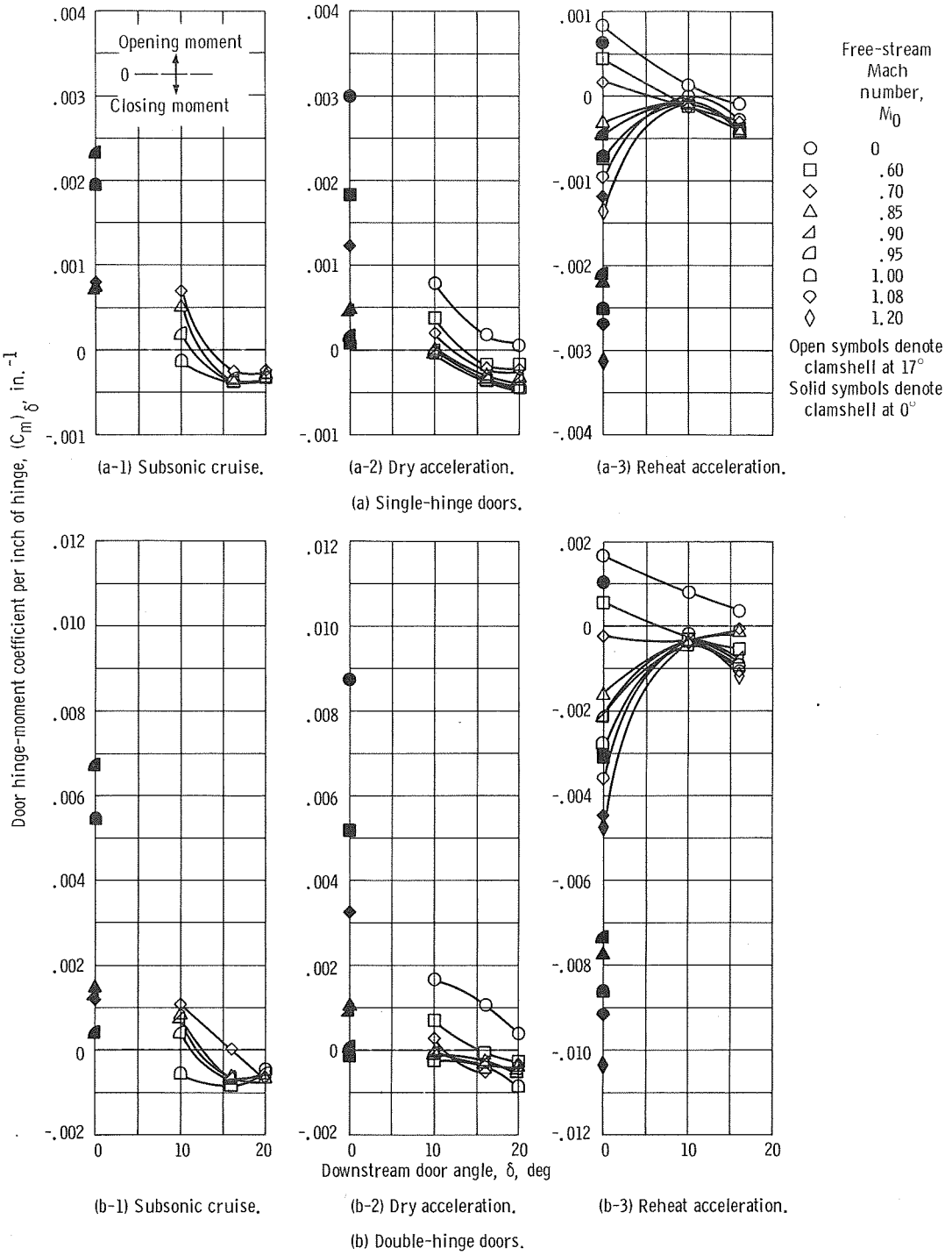

Figure 16. - Door hinge-moment coefficients. Corrected secondary-weight-flow ratio, $\omega\sqrt{\tau} = 0.04$.

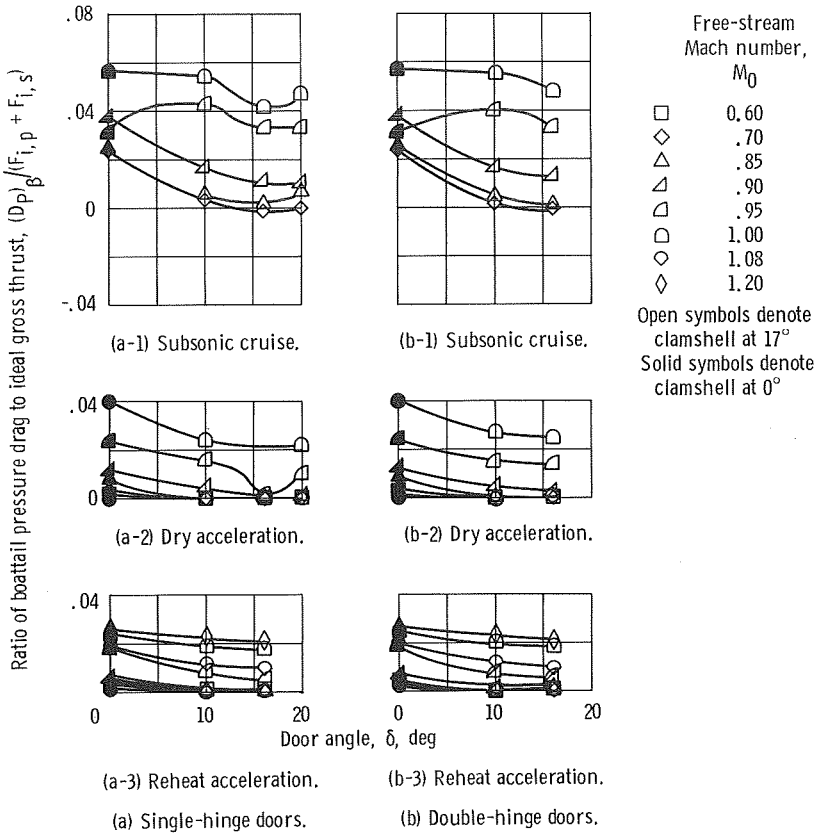

Figure 17. - Boattail pressure drag. Corrected secondary-weight-flow ratio, $\omega\sqrt{\tau} = 0.04$.

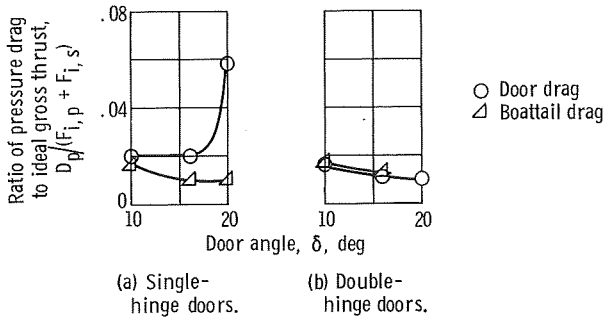

Figure 18. - Door and boattail pressure drag. Subsonic cruise; free-stream Mach number, 0.90; corrected secondary-weight-flow ratio, $\omega\sqrt{\tau} = 0.04$.

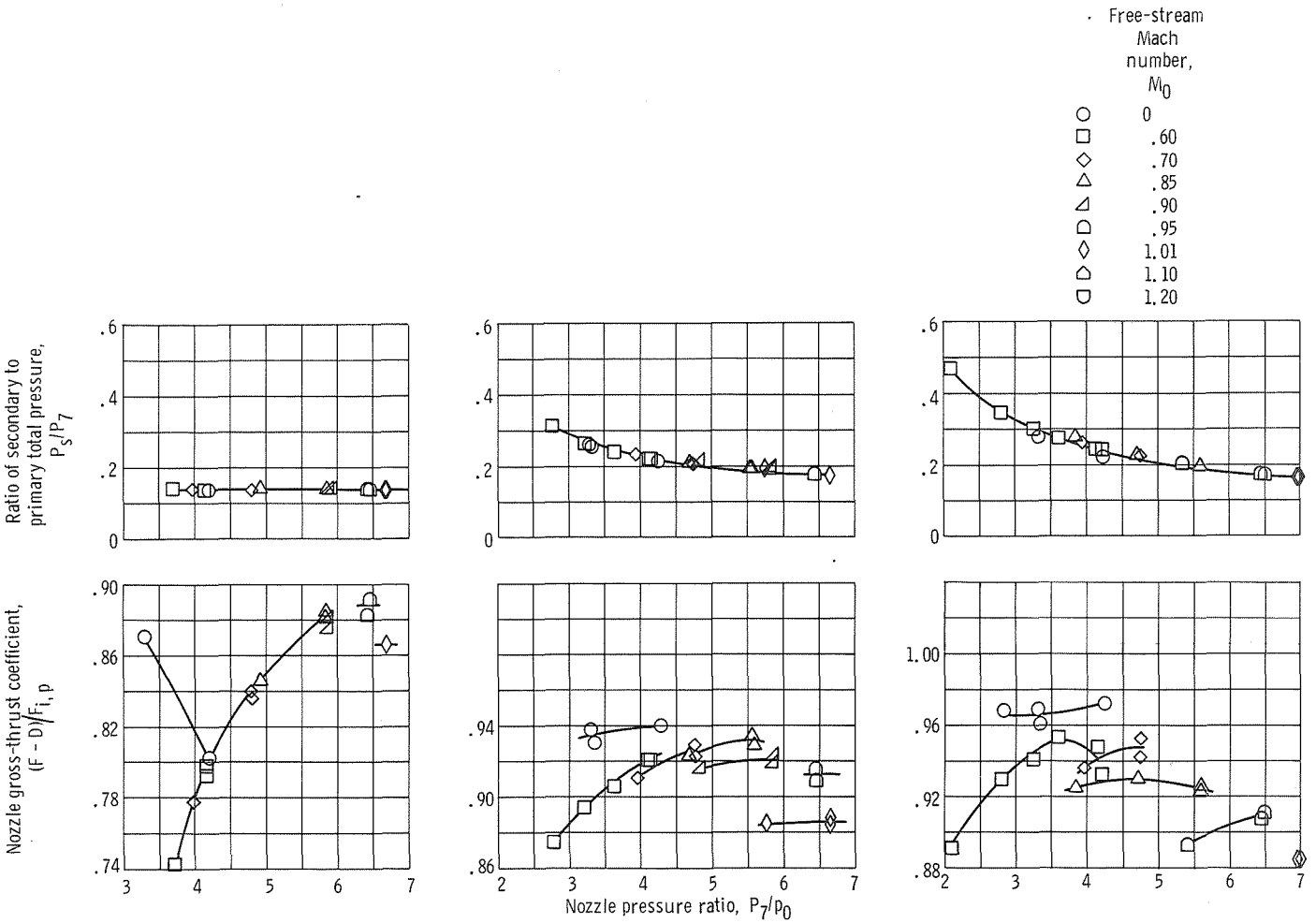

(a) Small primary nozzle; closed doors; clamshell at 0°; corrected secondary-weight-flow ratio, $\omega\sqrt{\tau} = 0.02$.

(b) Small primary nozzle; 10° single-hinge doors; clamshell at 17°; corrected secondary-weight-flow ratio, $\omega\sqrt{\tau} = 0.02$.

(c) Small primary nozzle; 16° single-hinge doors; clamshell at 17°; corrected secondary-weight-flow ratio, $\omega\sqrt{\tau} = 0.02$.

Figure 19. - Basic performance data as function of nozzle pressure ratio.

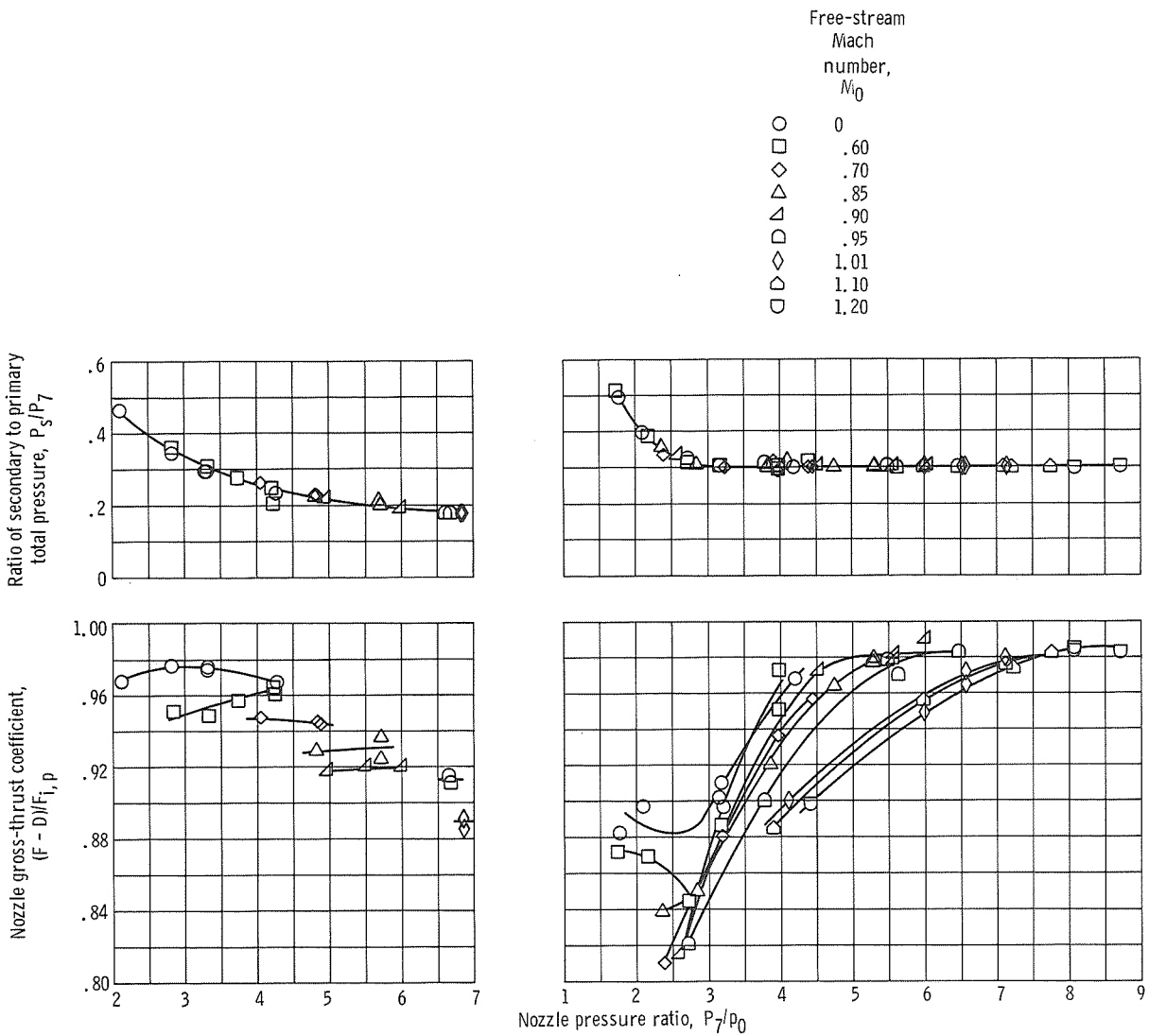

(d) Small primary nozzle; 20° single-hinge doors; clamshell at 17°; corrected secondary-weight-flow ratio, $\omega\sqrt{\tau} = 0.02$.

(e) Large primary nozzle; closed doors; clamshell at 0°; corrected secondary-weight-flow ratio, $\omega\sqrt{\tau} = 0.04$.

Figure 19. - Continued.

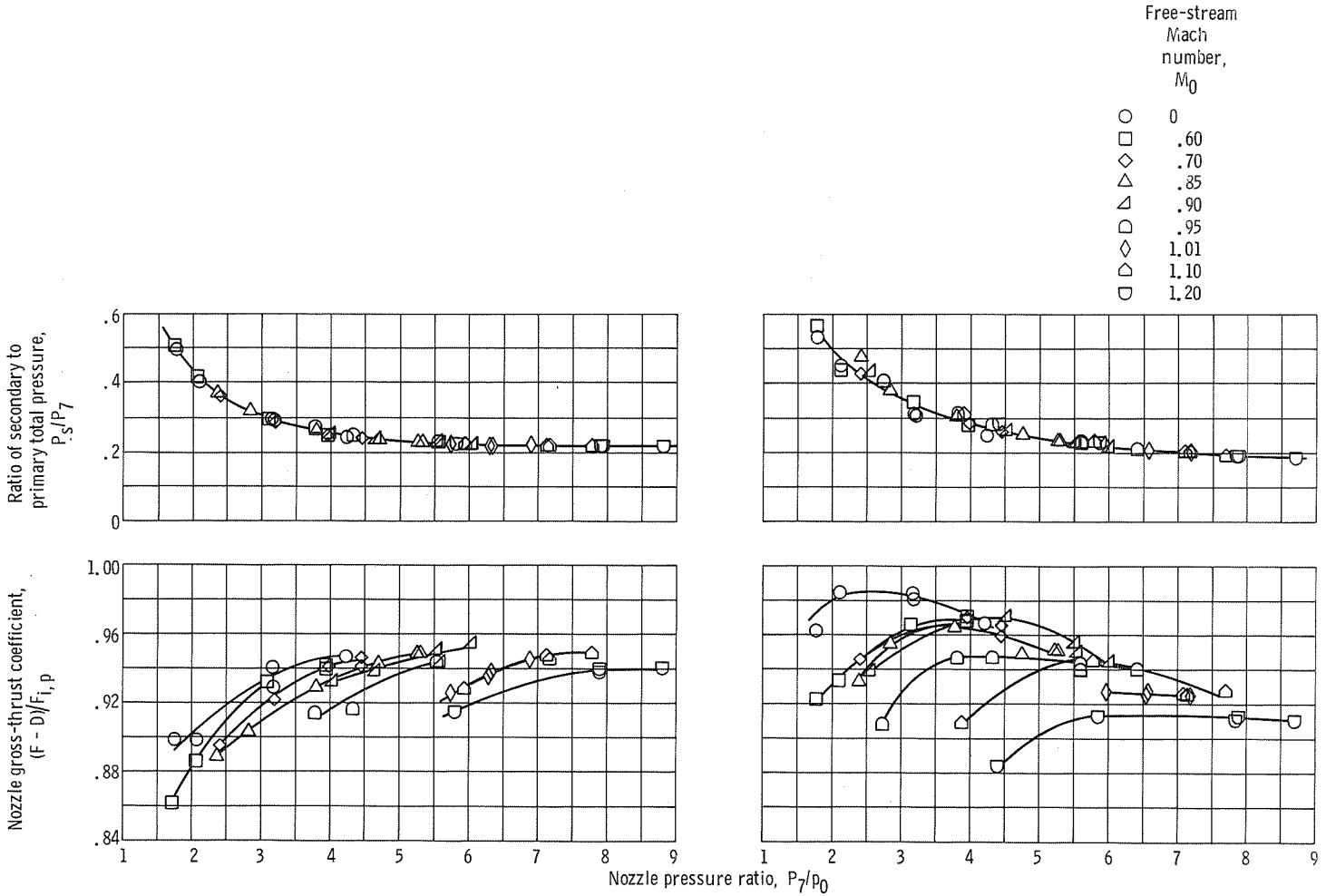

(f) Large primary nozzle; closed doors; clamshell at 17°; corrected secondary-weight-flow ratio, $\omega\sqrt{\tau} = 0.04$.

(g) Large primary nozzle; 10° single-hinge doors; clamshell at 17°; corrected secondary-weight-flow ratio, $\omega\sqrt{\tau} = 0.04$.

Figure 19. - Continued.

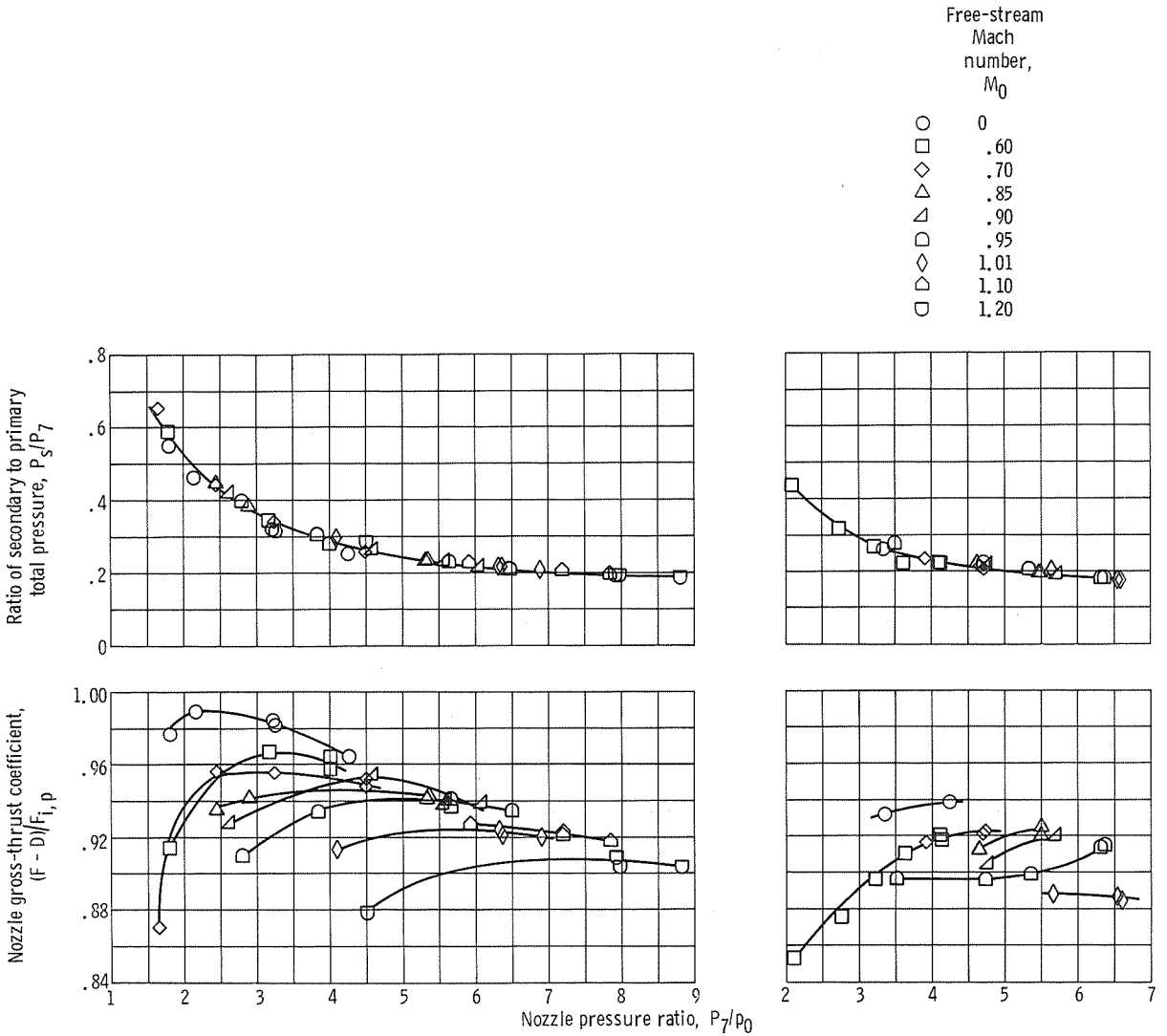

(h) Large primary nozzle; 16° single-hinge doors; clamshell at 17°; corrected secondary-weight-flow ratio, $\omega\sqrt{\tau} = 0.04$.

(i) Small primary nozzle; 5°-10° double-hinge doors; clamshell at 17°; corrected secondary-weight-flow ratio, $\omega\sqrt{\tau} = 0.02$.

Figure 19. - Continued.

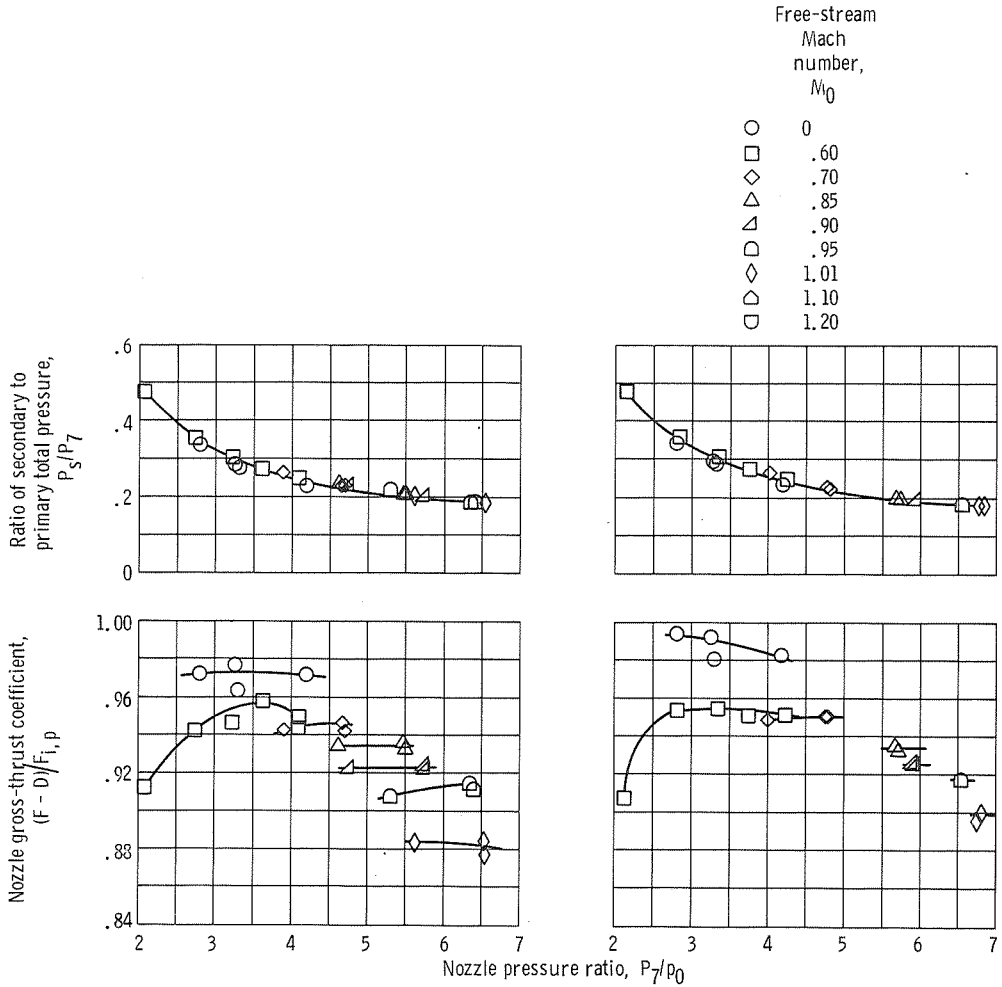

(j) Small primary nozzle; 8°-16° double-hinge doors; clamshell at 17°; corrected secondary-weight-flow ratio, $\omega\sqrt{\tau} = 0.02$.

(k) Small primary nozzle; 10°-20° double-hinge doors; clamshell at 17°; corrected secondary-weight-flow ratio, $\omega\sqrt{\tau} = 0.02$.

Figure 19. - Continued.

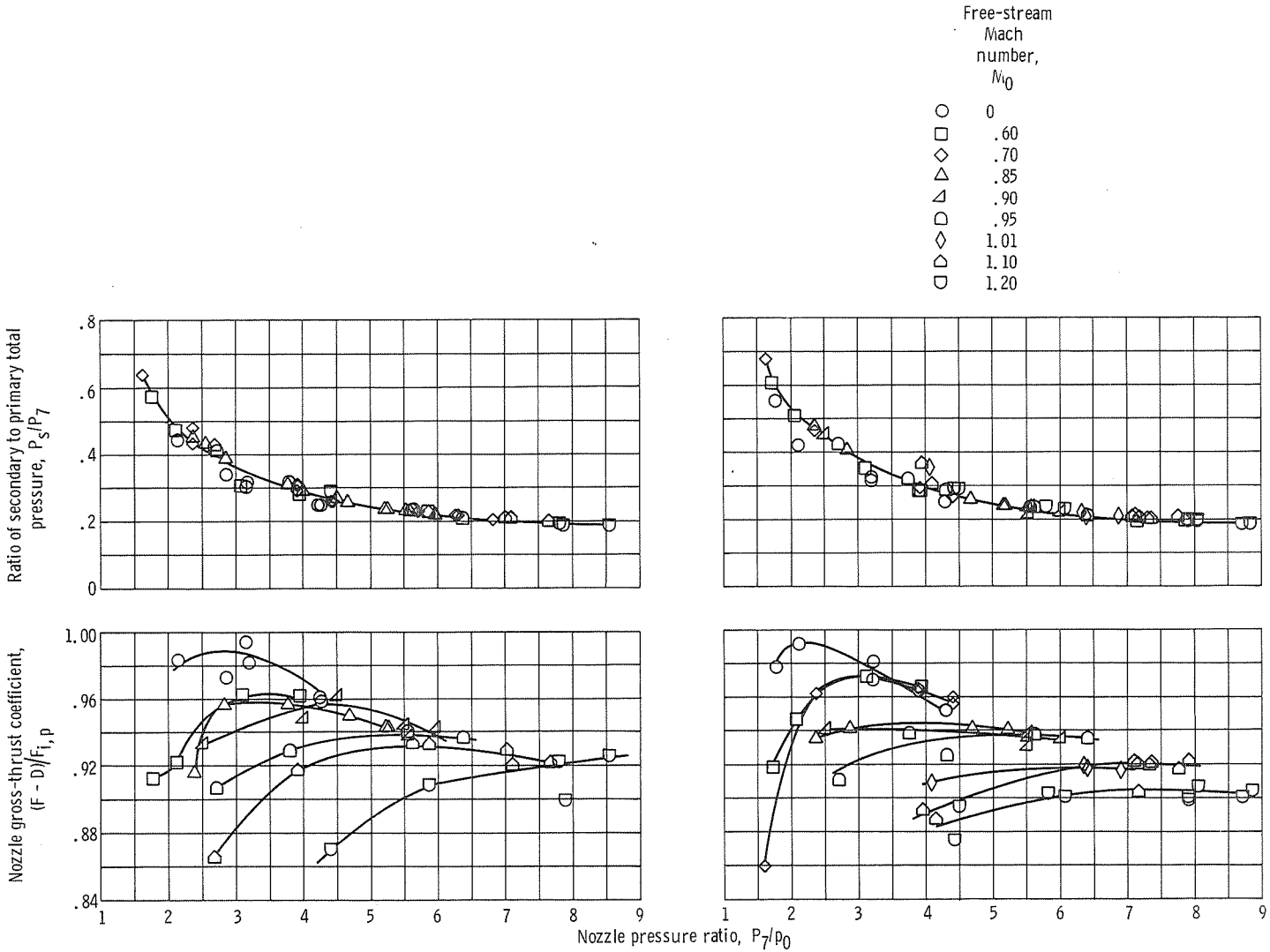

(l) Large primary nozzle; 5°-10° double-hinge doors; clamshell at 17°; corrected secondary-weight-flow ratio, $\omega\sqrt{\tau} = 0.04$.

(m) Large primary nozzle; 8°-16° double-hinge doors; clamshell at 17°; corrected secondary-weight-flow ratio, $\omega\sqrt{\tau} = 0.04$.

Figure 19. - Concluded.

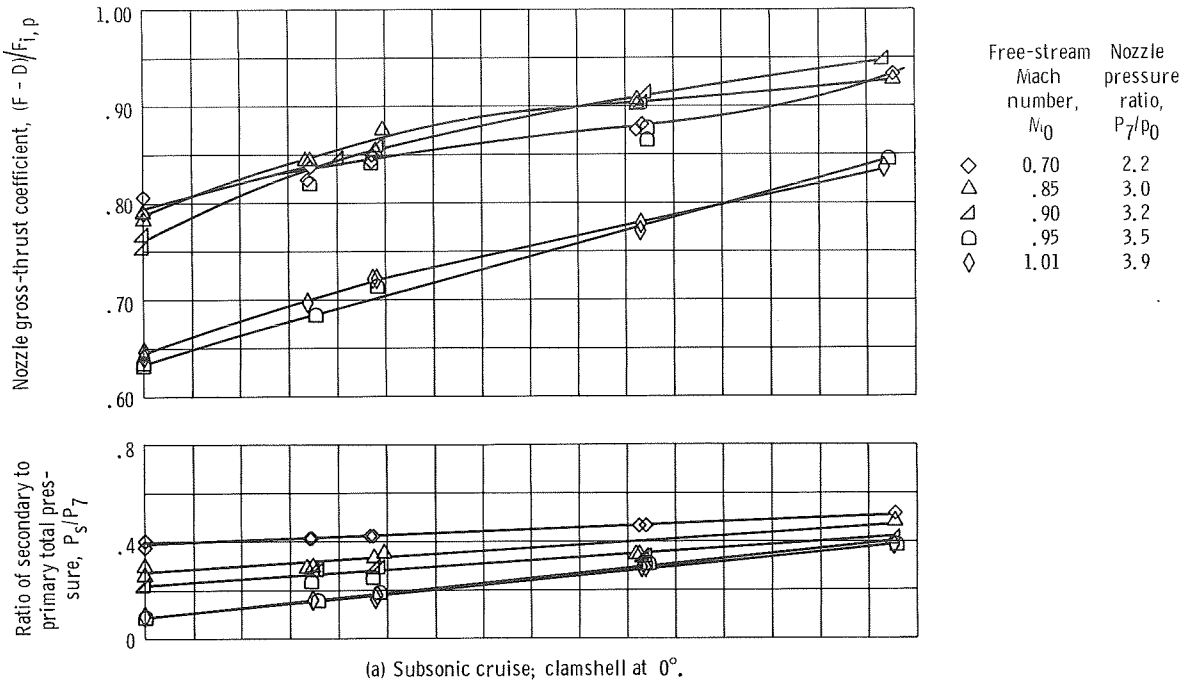

(a) Subsonic cruise; clamshell at 0°.

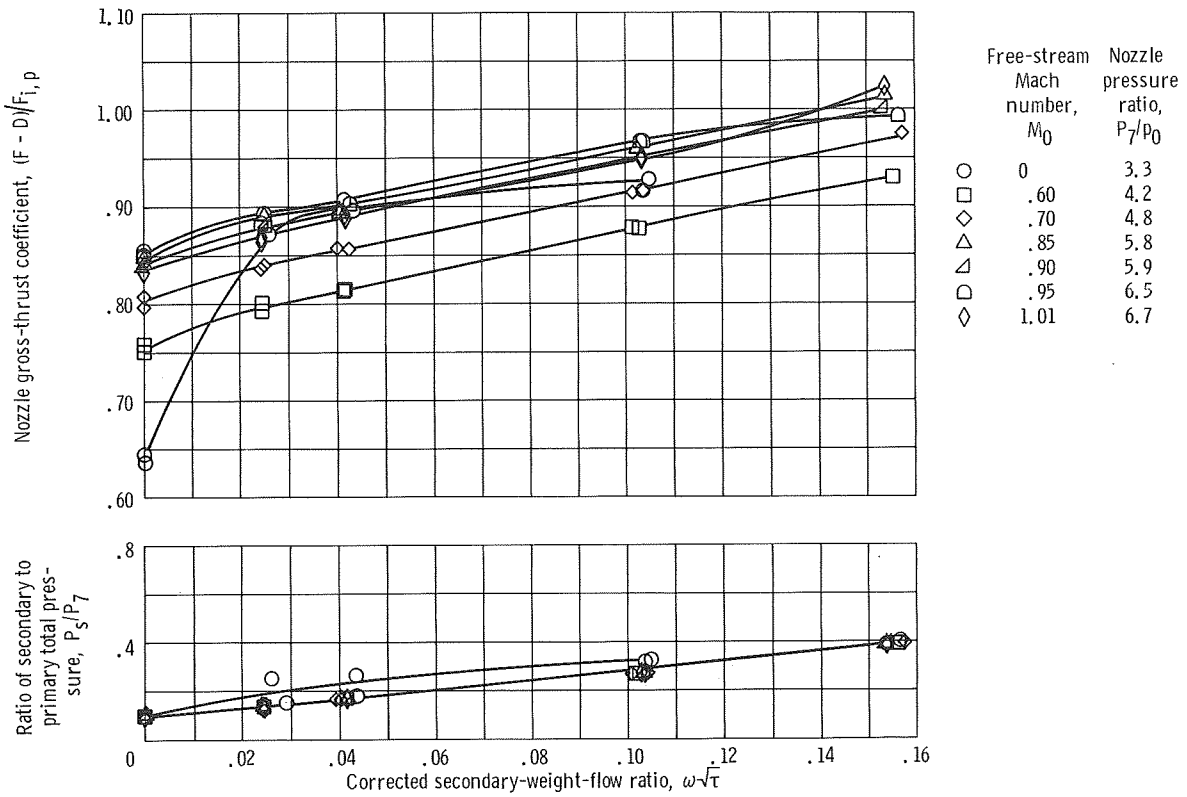

(b) Dry acceleration; clamshell at 0°.

Figure 20. - Basic performance data for closed-door configuration as function of corrected secondary-weight-flow ratio.

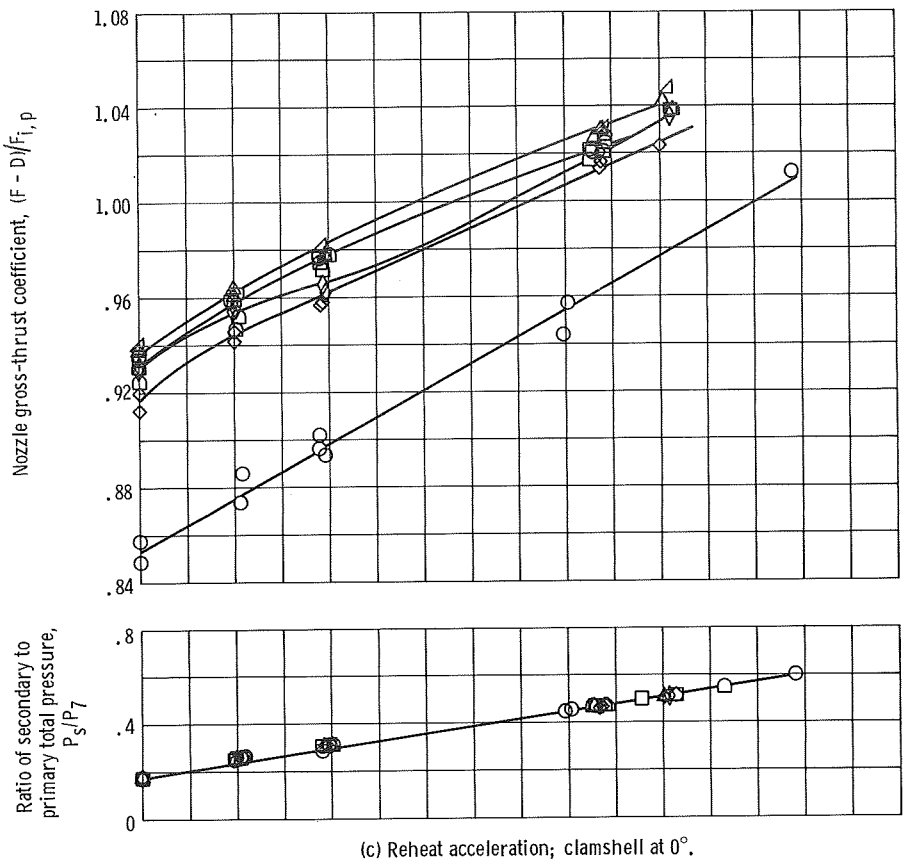

(c) Reheat acceleration; clamshell at 0°.

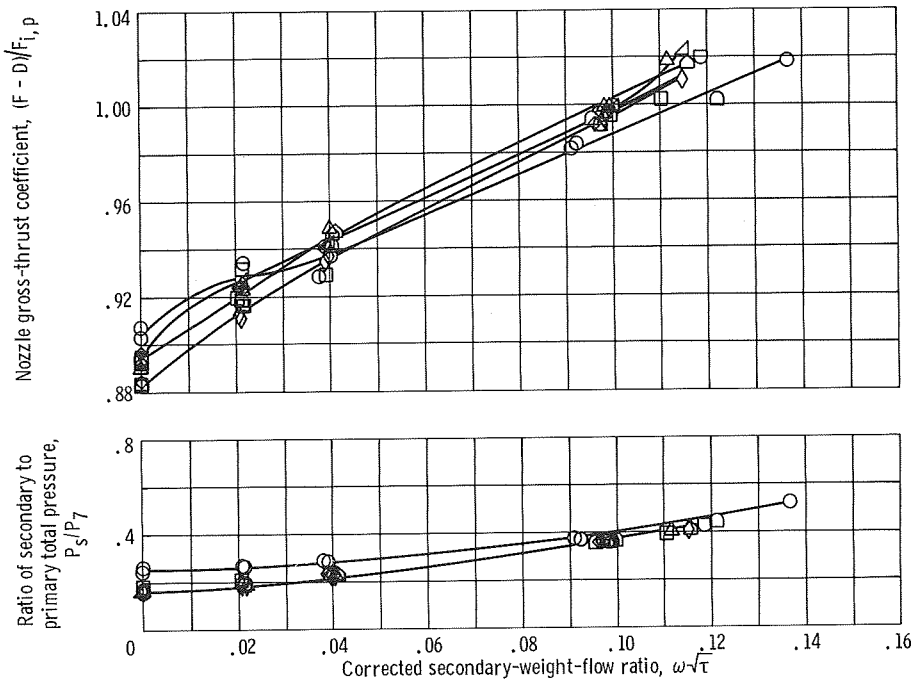

(d) Reheat acceleration; clamshell at 17°.

Figure 20. - Concluded.

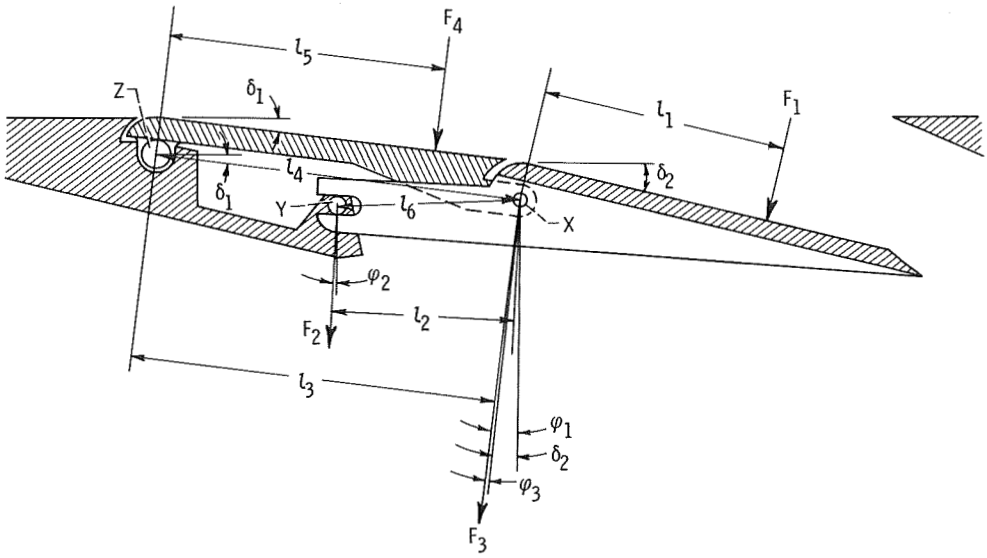

Figure 21. - Assumed mechanism for double-hinge-door analysis.

NASA-Langley, 1970 —— 28 E-5554

NATIONAL AERONAUTICS AND SPACE ADMINISTRATION
WASHINGTON, D. C. 20546
OFFICIAL BUSINESS

FIRST CLASS MAIL

POSTAGE AND FEES PAID
NATIONAL AERONAUTICS AN
SPACE ADMINISTRATION

POSTMASTER: If Undeliverable (Section 158
Postal Manual) Do Not Retur

"The aeronautical and space activities of the United States shall be conducted so as to contribute . . . to the expansion of human knowledge of phenomena in the atmosphere and space. The Administration shall provide for the widest practicable and appropriate dissemination of information concerning its activities and the results thereof."

—NATIONAL AERONAUTICS AND SPACE ACT OF 1958

NASA SCIENTIFIC AND TECHNICAL PUBLICATIONS

TECHNICAL REPORTS: Scientific and technical information considered important, complete, and a lasting contribution to existing knowledge.

TECHNICAL NOTES: Information less broad in scope but nevertheless of importance as a contribution to existing knowledge.

TECHNICAL MEMORANDUMS: Information receiving limited distribution because of preliminary data, security classification, or other reasons.

CONTRACTOR REPORTS: Scientific and technical information generated under a NASA contract or grant and considered an important contribution to existing knowledge.

TECHNICAL TRANSLATIONS: Information published in a foreign language considered to merit NASA distribution in English.

SPECIAL PUBLICATIONS: Information derived from or of value to NASA activities. Publications include conference proceedings, monographs, data compilations, handbooks, sourcebooks, and special bibliographies.

TECHNOLOGY UTILIZATION PUBLICATIONS: Information on technology used by NASA that may be of particular interest in commercial and other non-aerospace applications. Publications include Tech Briefs, Technology Utilization Reports and Notes, and Technology Surveys.

Details on the availability of these publications may be obtained from:

SCIENTIFIC AND TECHNICAL INFORMATION DIVISION
NATIONAL AERONAUTICS AND SPACE ADMINISTRATION
Washington, D.C. 20546